

INFRARED PROPERTIES OF CATAclySMIC VARIABLES IN THE 2 MICRON ALL-SKY SURVEY SECOND INCREMENTAL DATA RELEASE

D. W. HOARD AND S. WACHTER

Cerro Tololo Inter-American Observatory,¹ Casilla 603, La Serena, Chile; dhoard@noao.edu, swachter@noao.edu

L. LEE CLARK

Department of Astronomy, San Diego State University, San Diego, CA 92182; clark@bellus.sdsu.edu

AND

TIMOTHY P. BOWERS

Steward Observatory, University of Arizona, Tucson, AZ 85721; tbowers@physics.arizona.edu

Received 2001 July 29; accepted 2001 September 21

ABSTRACT

Cataclysmic variables (CVs) have “traditionally” been observed primarily at short wavelengths because accretion-generated luminosity, which peaks in the optical–ultraviolet, dominates the radiated energy of most systems. Hence, relatively little is known about their infrared (IR) properties. Investigating CVs in the IR will contribute to the understanding of key system components that are expected to radiate at these wavelengths, such as the cool outer disk, accretion stream, and secondary star. We have compiled the near-IR J , H , and K_s band photometry of all cataclysmic variables contained in the sky coverage of the Second Incremental Data Release of the 2 Micron All Sky Survey (2MASS). This data comprises 251 cataclysmic variables with reliably identified near-IR counterparts and $S/N > 10$ photometry in one or more of the three near-IR bands. In addition to tables containing the 2MASS data, we present a set of near-IR finding charts for selected systems. A comparison between the 2MASS photometry and various literature sources of near-IR photometry of cataclysmic variables shows good agreement after allowing for differences in photometric systems and the intrinsic variability of cataclysmic variables. The bulk of our analysis consists of an exploration of near-IR color-color diagrams of the main cataclysmic variable classes. Results from this analysis include: (1) dwarf novae in outburst and quiescence occupy distinct regions of their color-color diagram; (2) nova-like CVs (and dwarf novae in outburst) have colors similar to F–K main-sequence stars, although this does not imply that they have F–K type secondary stars; (3) polars and intermediate polars also occupy distinct regions in their color-color diagram, with most polars having colors essentially indistinguishable from late (M0+) main-sequence stars; (4) there is no strong correlation between age and color for novae, except that many old novae (> 75 yr since outburst) have colors similar to F–K main-sequence stars; and (5) there are unusual and unexplained loci of data points in all the color-color diagrams that warrant further investigation in the IR. Except in the case of the polars, near-IR photometry of cataclysmic variables does *not* isolate the luminosity contribution of their secondary stars. In general, the near-IR colors of cataclysmic variables are significantly and systematically offset blueward of the spectral type of secondary star expected at their orbital periods. This blue contamination of the near-IR light almost certainly originates from the accretion process. For a few systems, their near-IR color is redder than the secondary star expected at their orbital period. One effect that can explain some, but not all, of the red-excess cataclysmic variables is the presence of an evolved secondary star. We suggest that this can also be caused by the luminosity contribution of the cool outer regions of prominent accretion disks. There is at least a weak trend of redder color in higher inclination systems (in which the disk rim would be most visible and most obscure the hot inner region) that supports this hypothesis.

Subject headings: accretion, accretion disks — infrared: stars — novae, cataclysmic variables — stars: dwarf novae — stars: fundamental parameters — surveys

On-line material: machine-readable tables

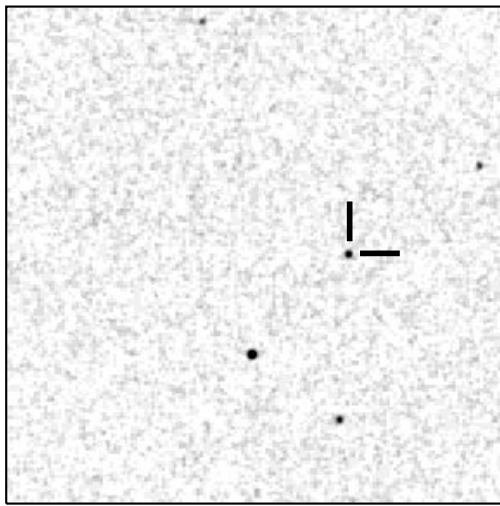
1. INTRODUCTION

1.1. *Cataclysmic Variables*

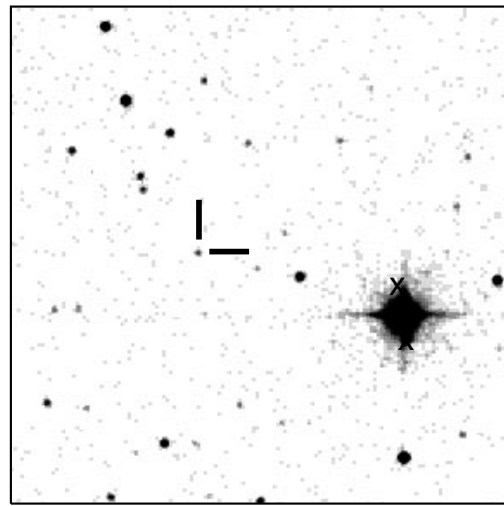
Cataclysmic variables (CVs) are semidetached interacting binary stars composed of a white dwarf (WD) primary star and a low-mass ($\lesssim 1 M_\odot$), usually main-sequence, secondary star, with typical orbital periods of $\lesssim 1$ day. The Roche-lobe-filling secondary star loses mass through the inner

Lagrangian point into an accretion disk formed around the WD (for nonmagnetic CVs). Viscous interactions in the disk cause matter to spiral inward until it accretes onto the WD. Nonmagnetic CVs are divided into three main classes: dwarf novae (CVs in which a disk instability causes quasi-periodic outbursts that temporarily increase the optical brightness by ~ 2 – 10 mag), nova-like CVs (CVs characterized by an approximately constant, high rate of mass transfer, a prominent disk, and bright luminosity), and novae (CVs in which a thermonuclear runaway is ignited in the reservoir of accreted material on the WD, releasing $\sim 10^{46}$ ergs in ~ 1 yr).

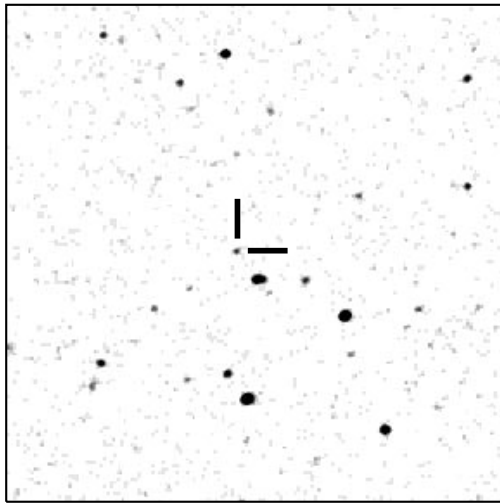
¹ Operated by the Association of Universities for Research in Astronomy, Inc., under cooperative agreement with the National Science Foundation.



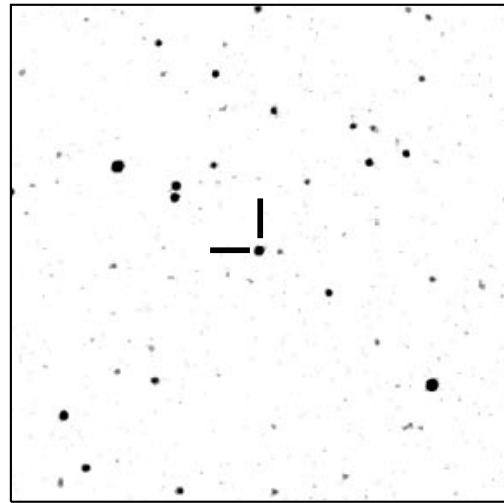
XY Ari



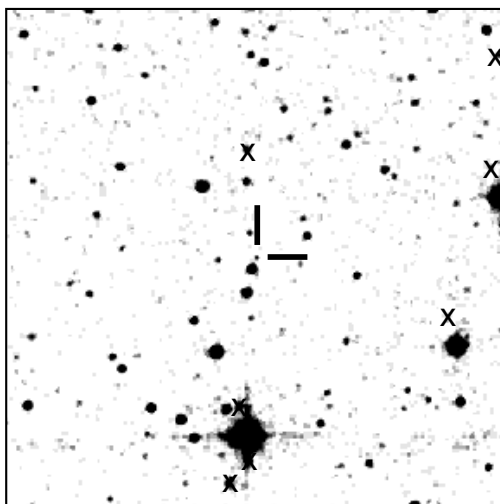
Cam (05:57:24, +72:41:52) J



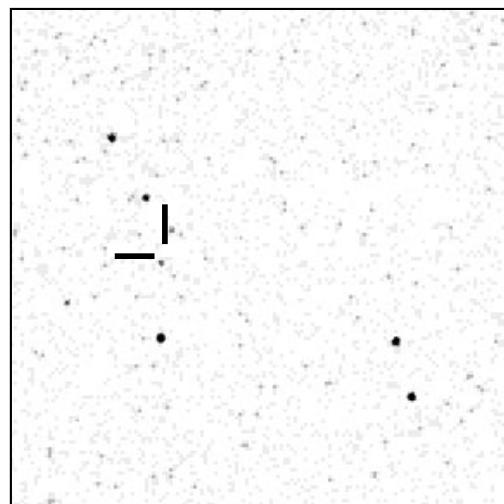
Cam (05:58:18, +67:53:46)



PU CMa

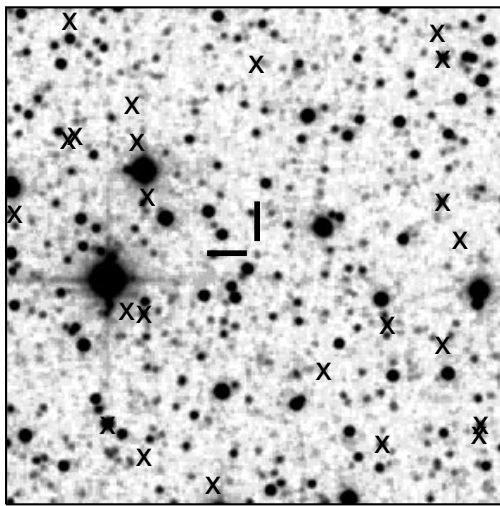


V452 Cas

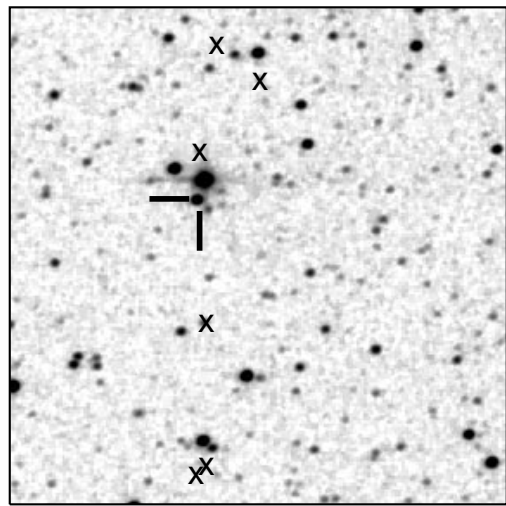


AL Com J X

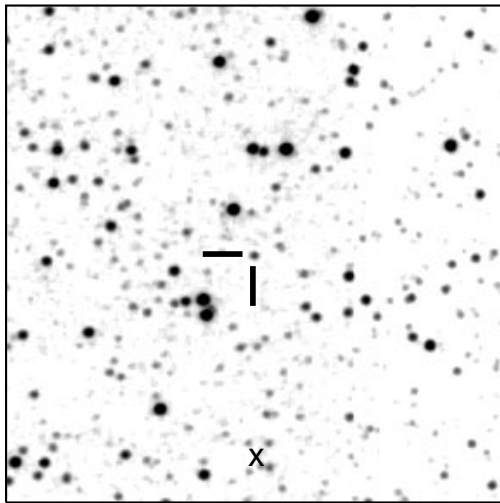
FIG. 1.—2MASS image finding charts for selected CVs. The charts measure $5' \times 5'$; north is at the top and east is to the left. See § 2.1 for the key to symbols and annotations.



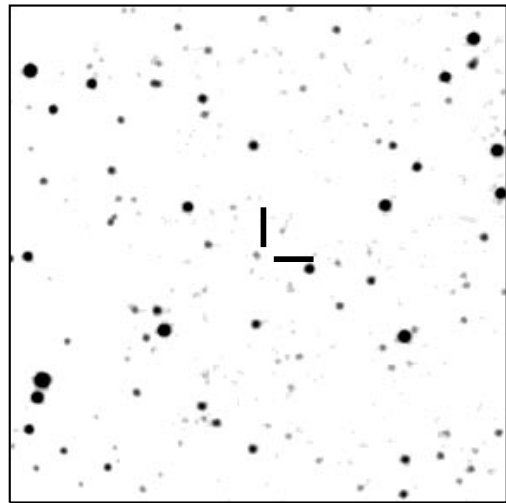
Cyg (19:58:14, +32:32:42)



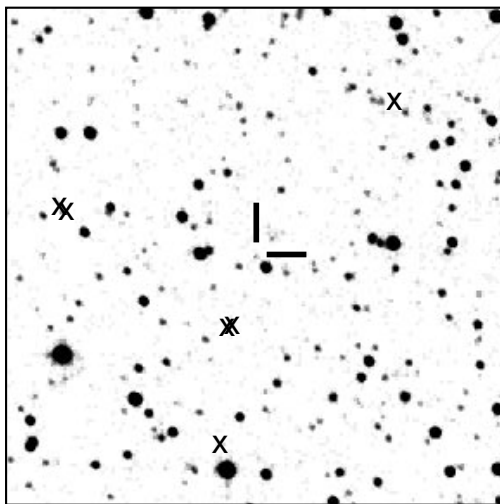
Cyg (21:30:18, +47:10:07)



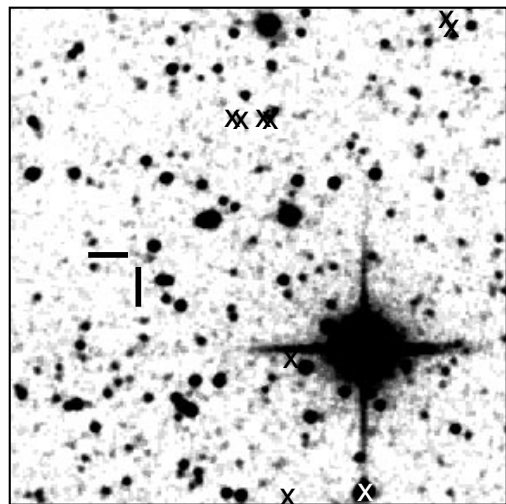
EY Cyg



V450 Cyg

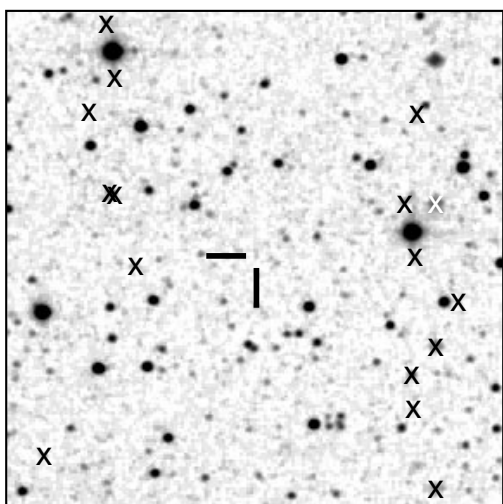


V503 Cyg

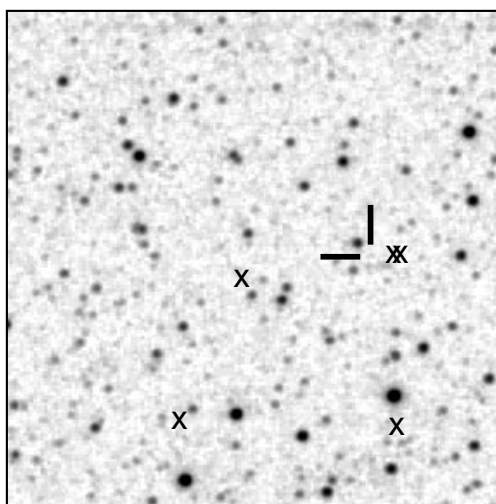


V823 Cyg

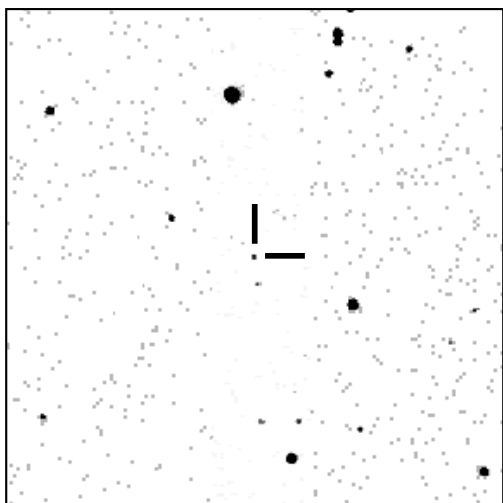
FIG. 1.—Continued



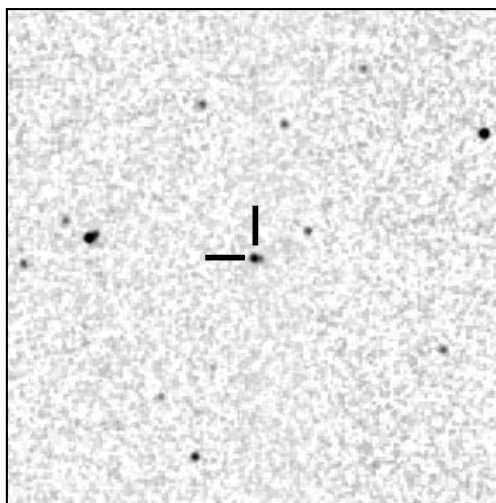
V1114 Cyg ?



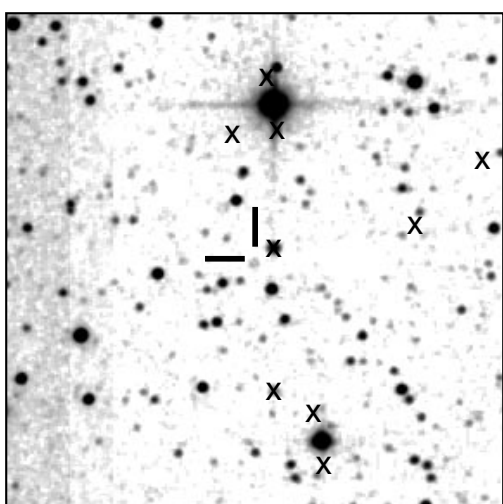
V1819 Cyg x



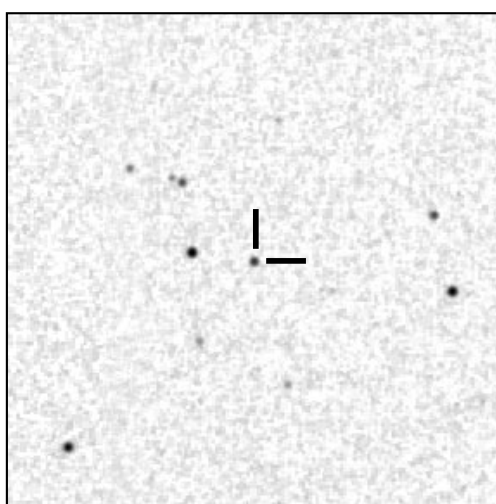
Eri (03:54:10, -16:52:50) J



PQ Gem

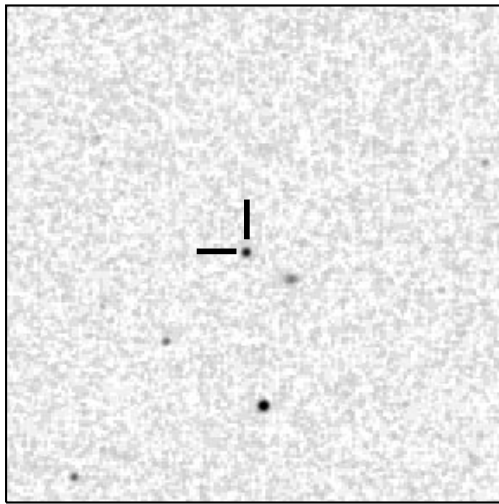


V446 Her ?

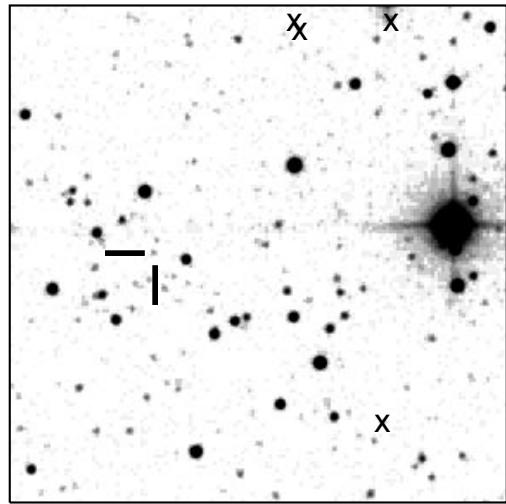


Leo (09:24:56, +13:20:52)

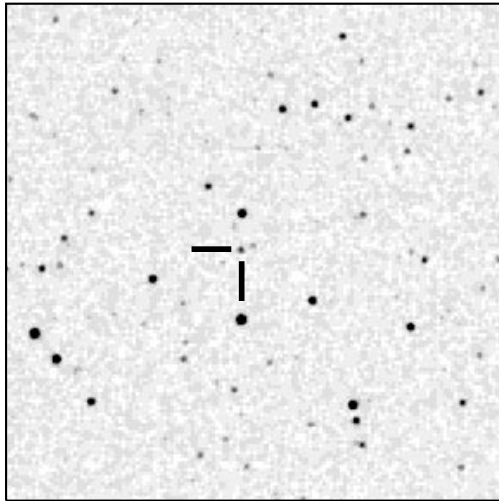
FIG. 1.—Continued



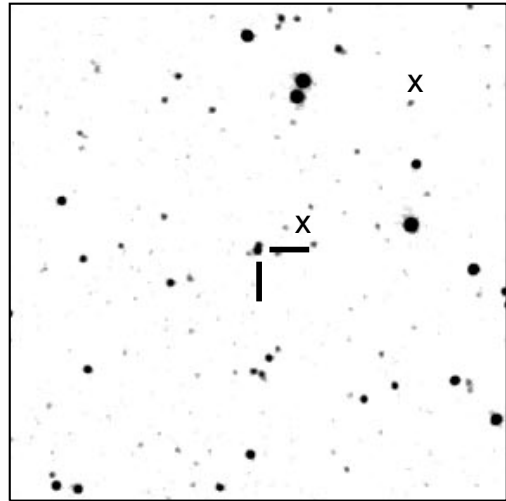
LMi (10:26:27, +38:45:01)



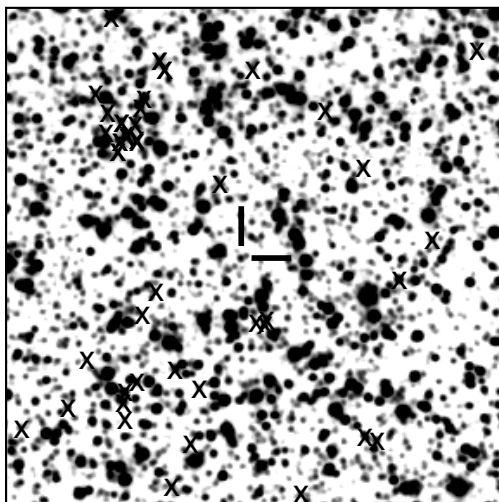
V369 Lyr J



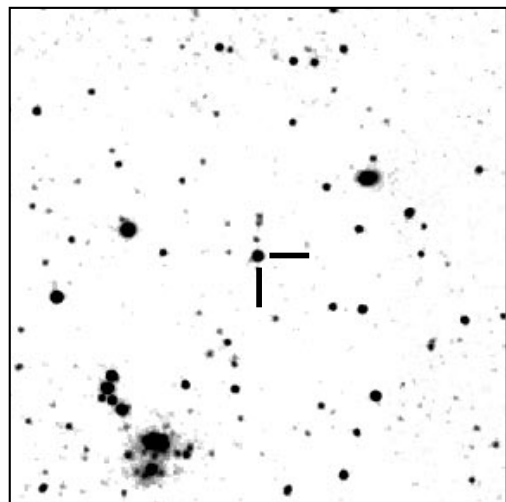
AD Men J



KQ Mon

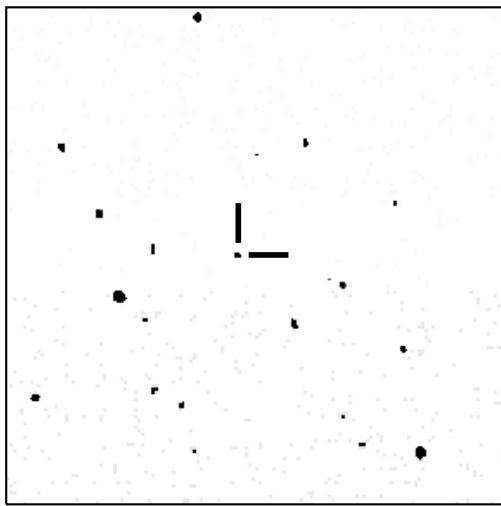


V972 Oph

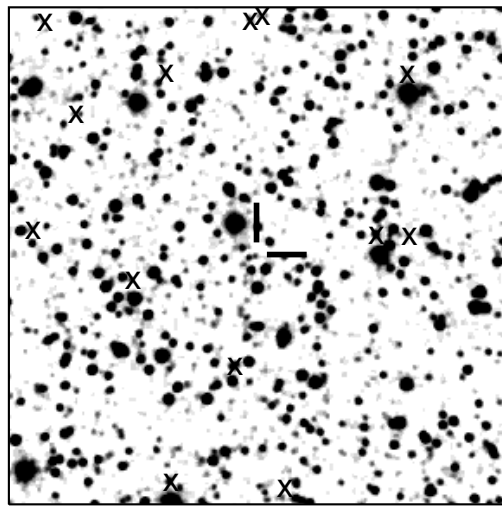


V529 Ori

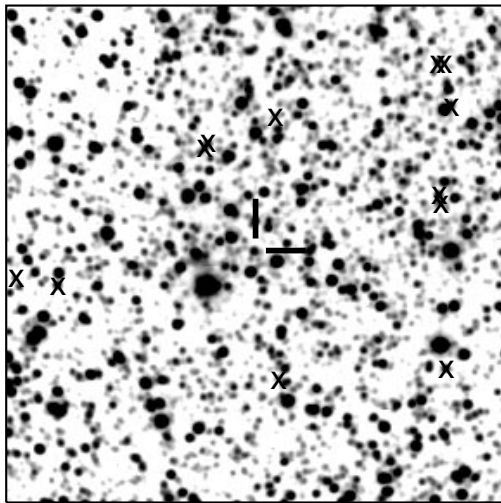
FIG. 1.—Continued



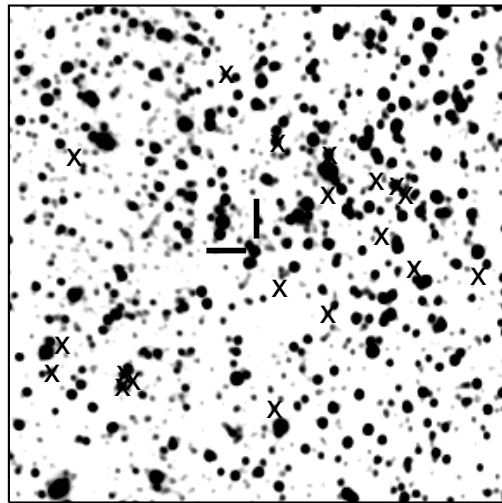
V367 Peg J



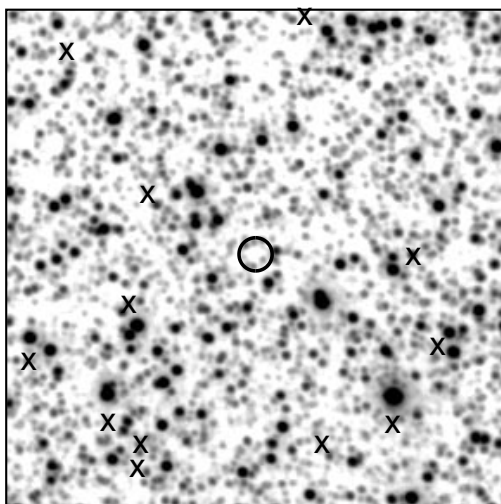
GR Sgr



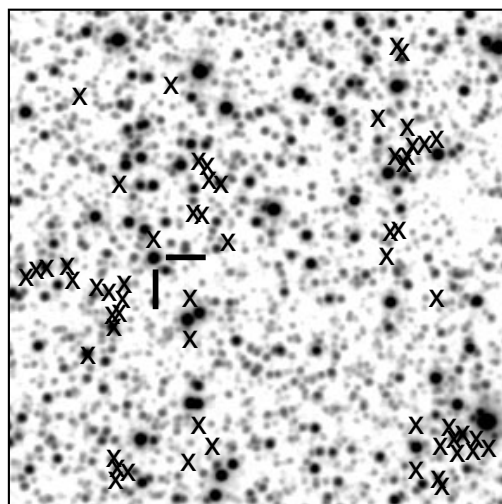
V732 Sgr



V759 Sgr ?

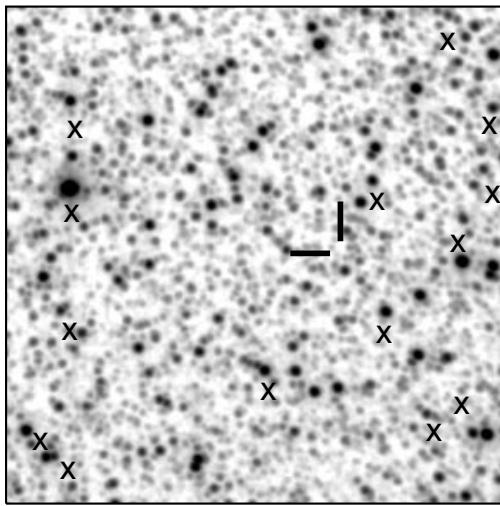


V990 Sgr ?

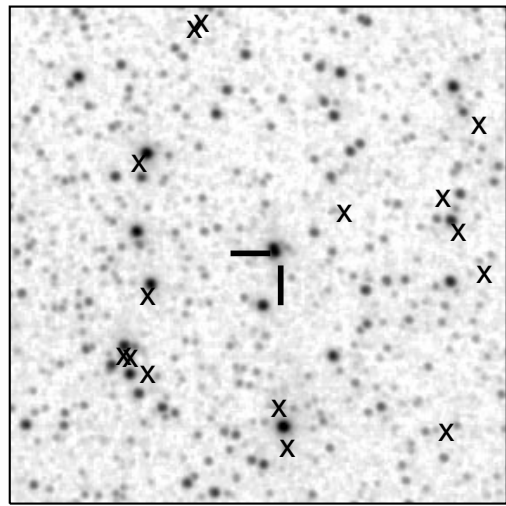


V2468 Sgr

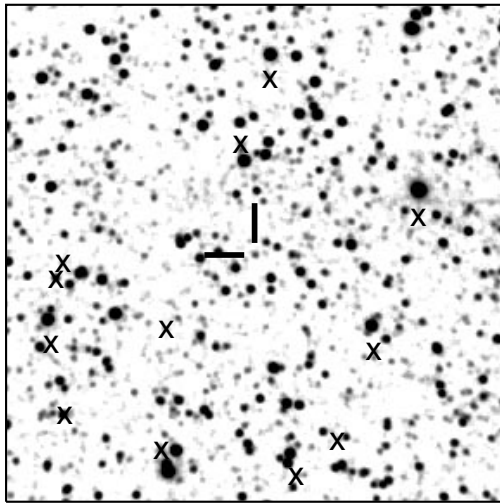
FIG. 1.—Continued



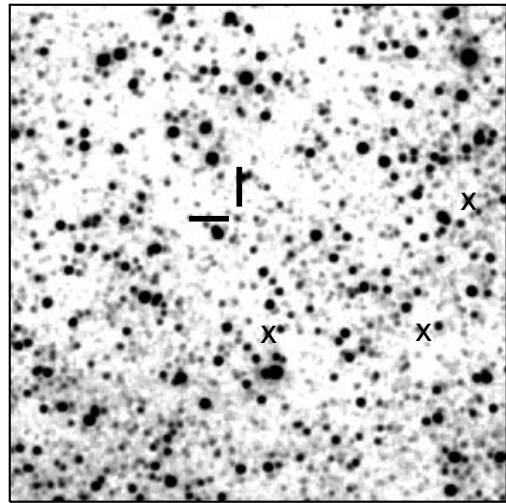
V3889 Sgr x



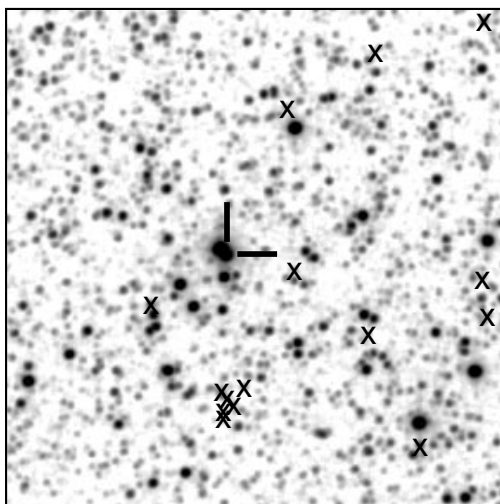
V4074 Sgr ?



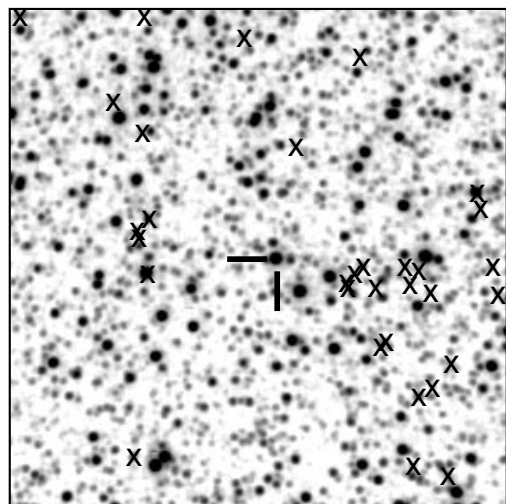
V4362 Sgr



V478 Sco



V734 Sco



V745 Sco

FIG. 1.—Continued

TABLE 1
CVs IN THE 2MASS SECOND INCREMENTAL DATA RELEASE

| Name (1) | R.A. (2000) (2) | Decl. (2000) (3) | Offset (arcsec) (4) | Type (5) | P_{orb} (days) (6) | J (mag) (7) | H (mag) (8) | K_s (mag) (9) | Notes (10) |
|-----------------|-----------------------|------------------------|---------------------------|-------------|-----------------------------------|---------------------|---------------------|-----------------------|--------------------|
| WW Cet | 00 11 24.8 | -11 28 43 | 0.25 | ugz: | 0.1758 | 11.081 (26) | 10.939 (27) | 10.825 (26) | ... |
| VW Tuc | 00 20 19.1 | -73 52 08 | 0.09 | UG: | ... | 15.869 (82) | 15.597 (132) | 15.355 (193) | ... |
| And | 00 21 48.6 | 35 04 51 | 1.30 | cv | ... | 14.029 (33) | 13.807 (51) | 13.740 (48) | ... |
| Psc 3 | 00 24 52.5 | -01 53 35 | 0.20 | ug: | ... | 13.471 (27) | 12.290 (31) | 11.096 (27) | ... |
| PX And | 00 30 05.8 | 26 17 27 | 0.25 | nl/vy | 0.146353 | 14.652 (39) | 14.506 (50) | 14.339 (62) | ... |
| HQ And | 00 31 35.9 | 43 49 05 | 0.27 | cv | ... | 15.259 (47) | 15.188 (92) | 15.113 (130) | ... |
| HV And | 00 40 55.3 | 43 24 59 | 0.43 | nl | 0.05599 | 15.363 (49) | 15.141 (84) | 15.134 (126) | ... |
| And | 00 41 23.7 | 41 15 00 | 1.06 | UG: | ... | 15.303 (60) | 14.780 (84) | 14.394 (89) | ... |
| V452 Cas | 00 52 18.0 | 53 51 51 | 0.77 | ugsu | ... | 15.904 (75) | 15.623 (141) | 15.298 (148) | ... |
| IW And | 01 01 08.9 | 43 23 26 | 0.11 | ux | ... | 14.997 (41) | 14.690 (60) | 14.567 (82) | ... |
| RX And | 01 04 35.6 | 41 17 58 | 0.22 | ugz | 0.209893 | 10.520 (28) | 10.390 (28) | 10.304 (31) | ... |
| Cet 7 | 01 09 34.8 | -08 00 33 | 0.97 | nl: | ... | 13.686 (26) | 13.412 (31) | 12.758 (34) | ... |
| FO And | 01 15 32.1 | 37 37 35 | 0.49 | ugsu | 0.07161 | 15.460 (51) | 15.634 (128) | 15.015 (114) | ... |
| EQ Cet | 01 28 52.3 | -23 39 44 | 3.26 | am | ... | 16.733 (156) | 16.389 (237) | 15.768 (252) | ... |
| TW Tri | 01 36 37.0 | 32 00 40 | 0.13 | cv/UGZ | 0.207584 | 14.552 (40) | 13.981 (40) | 13.666 (45) | ... |
| KT Per | 01 37 08.7 | 50 57 20 | 0.71 | ugz | 0.162658 | 13.307 (28) | 12.804 (30) | 12.596 (30) | ... |
| TX Tri | 01 37 37.2 | 30 02 49 | 0.37 | ugss | ... | 15.023 (40) | 14.577 (58) | 14.503 (78) | ... |
| BL Hyi | 01 41 00.3 | -67 53 28 | 0.81 | am | 0.078915 | 14.315 (36) | 13.638 (38) | 13.250 (46) | ... |
| AR And | 01 45 03.3 | 37 56 33 | 0.07 | ug | 0.163 | 14.607 (31) | 13.979 (43) | 13.745 (46) | ... |
| AI Tri | 02 03 48.6 | 29 59 26 | 0.35 | am | 0.191745 | 14.211 (31) | 13.939 (40) | 13.617 (47) | ... |
| BO Cet | 02 06 39.2 | -02 03 43 | 0.68 | nl | ... | 14.041 (27) | 13.837 (34) | 13.606 (46) | ... |
| TT Ari | 02 06 53.1 | 15 17 43 | 0.89 | vy/dq: | 0.137551 | 10.980 (25) | 10.923 (29) | 10.850 (33) | ... |
| LX And | 02 19 44.1 | 40 27 23 | 0.61 | ug | ... | 14.698 (36) | 14.341 (44) | 14.020 (54) | ... |
| RW Tri | 02 25 36.1 | 28 05 51 | 0.51 | ux | 0.231883 | 11.931 (30) | 11.570 (31) | 11.434 (31) | * |
| FS And | 02 25 55.1 | 37 34 06 | 0.59 | ug | ... | 15.917 (69) | 15.663 (121) | 15.390 (167) | ... |
| KW And | 02 35 18.0 | 41 14 02 | 0.64 | UG | ... | 16.287 (114) | 15.708 (161) | > 15.022 | rd220 bl110 |
| Cet 5 | 02 35 40.4 | -13 21 12 | 0.35 | UG: | ... | 17.144 (186) | 15.858 (148) | > 16.171 | rd220 bl110 |
| PT Per | 02 42 51.2 | 56 41 31 | 0.29 | ug | ... | 15.013 (47) | 14.470 (53) | 14.310 (76) | ... |
| XY Ari | 02 56 08.1 | 19 26 34 | 1.21 | dq | 0.252697 | 16.124 (77) | 14.256 (41) | 13.381 (35) | * |
| Per | 03 09 13.6 | 33 31 27 | 4.46 | cv: | ... | 12.461 (38) | 11.894 (38) | 11.623 (33) | ... |
| EF Eri | 03 14 13.0 | -22 35 41 | 3.39 | am | 0.056266 | 17.184 (255) | 15.646 (144) | 15.343 (175) | high proper motion |
| VY For | 03 32 04.6 | -25 56 55 | 0.56 | am | 0.1586 | 15.585 (53) | 15.027 (75) | 14.853 (130) | ... |
| UZ For | 03 35 28.6 | -25 44 23 | 0.95 | am | 0.087865 | 15.337 (45) | 14.900 (75) | 14.782 (126) | ... |
| Eri | 03 54 10.2 | -16 52 50 | 1.72 | am: | ... | 16.448 (125) | 16.458 (268) | > 15.849 | rd220 bl110 * |
| VW Hyi | 04 09 11.3 | -71 17 41 | 0.44 | ugsu | 0.074271 | 12.562 (27) | 12.070 (37) | 11.752 (32) | ... |
| AH Eri | 04 22 38.1 | -13 21 30 | 0.41 | ug/dq:: | 0.2391 | 15.932 (71) | 15.366 (104) | 14.967 (121) | * |
| BF Eri | 04 39 29.8 | -04 35 57 | 2.32 | ug | ... | 12.961 (34) | 12.646 (35) | 12.574 (31) | ... |
| TU Men | 04 41 40.7 | -76 36 46 | 0.26 | ugsu | 0.1172 | 14.960 (44) | 14.310 (67) | 14.014 (79) | ... |
| FY Per | 04 41 56.6 | 50 42 36 | 0.54 | ux/ugz | ... | 11.776 (23) | 11.461 (30) | 11.327 (28) | ... |
| HV Aur | 04 53 16.8 | 38 16 29 | 0.88 | ugsu | 0.0823 | 13.619 (23) | 13.423 (33) | 13.284 (39) | ... |
| Tau 4 | 05 02 50.8 | 16 24 23 | 1.42 | cv | ... | 16.496 (119) | 15.543 (102) | 14.661 (92) | ... |
| AQ Eri | 05 06 13.0 | -04 08 07 | 1.14 | ugsu | 0.06094 | 16.468 (115) | 15.630 (113) | 15.594 (207) | ... |
| UU Col | 05 12 13.1 | -32 41 39 | 1.62 | dq | 0.144 | 16.874 (140) | > 16.233 | > 16.054 | rd200 bl100 |
| V1193 Ori | 05 16 26.7 | 00 12 14 | 0.39 | ux | 0.165 | 13.559 (26) | 13.453 (30) | 13.388 (43) | ... |
| ZZ Lep | 05 27 28.2 | -12 41 50 | ... | nl: | ... | ... | ... | ... | too bright |
| QZ Aur | 05 28 34.0 | 33 18 23 | 1.17 | na | 0.357496 | 15.811 (71) | 15.255 (93) | 15.006 (109) | ... |
| V1159 Ori | 05 28 59.5 | -03 33 53 | 0.96 | ugsu | 0.062178 | 13.823 (28) | 13.785 (34) | 13.679 (51) | ... |
| TV Col | 05 29 25.5 | -32 49 05 | 1.23 | dq | 0.228599 | 13.205 (28) | 12.826 (30) | 12.692 (33) | * |
| T Aur | 05 31 59.1 | 30 26 45 | 0.43 | nb | 0.204378 | 13.973 (36) | 13.715 (41) | 13.574 (38) | ... |
| V363 Aur | 05 33 33.5 | 36 59 32 | 0.39 | nl/ux | 0.321242 | 13.299 (30) | 12.964 (29) | 12.769 (41) | ... |
| V421 Tau | 05 48 22.9 | 22 42 02 | 0.36 | ug | ... | 15.945 (81) | 15.312 (118) | 15.390 (164) | ... |
| CN Ori | 05 52 07.8 | -05 25 01 | 0.34 | ugz | 0.163199 | 13.820 (29) | 13.317 (28) | 13.112 (35) | ... |
| Cam | 05 57 23.9 | 72 41 52 | 0.53 | dq | ... | 16.105 (96) | 16.084 (228) | 15.594 (217) | * |
| Cam | 05 58 18.0 | 67 53 46 | 0.50 | cv | ... | 15.139 (47) | 14.748 (59) | 14.762 (101) | * |
| V529 Ori | 05 58 22.3 | 20 15 26 | 0.73 | n:: | ... | 13.503 (30) | 12.169 (31) | 11.211 (34) | * |
| Cam 1 | 06 00 02.0 | 77 51 31 | 0.26 | cv: | ... | 15.754 (83) | 15.512 (152) | 15.479 (217) | ... |
| AD Men | 06 04 28.6 | -71 25 16 | 0.46 | ugSS | ... | 15.333 (46) | 14.923 (74) | 15.036 (171) | ... |
| Gem 1 | 06 10 43.9 | 25 10 32 | 0.74 | nl/ug? | ... | 13.107 (28) | 12.730 (32) | 12.623 (33) | ... |
| V344 Ori | 06 15 18.9 | 15 31 00 | 0.98 | ug: | ... | 15.787 (70) | 15.164 (78) | 14.737 (104) | ... |
| KR Aur | 06 15 43.9 | 28 35 09 | 0.35 | vy | 0.1628 | 16.236 (91) | 15.540 (105) | 15.784 (201) | ... |
| CZ Ori | 06 16 43.2 | 15 24 12 | 0.47 | ug | 0.2189 | 12.576 (31) | 12.381 (31) | 12.272 (36) | ... |
| RR Pic | 06 35 36.1 | -62 38 24 | 0.61 | nb | 0.145025 | 12.509 (30) | 12.397 (30) | 12.354 (36) | ... |
| KN Gem | 06 35 53.9 | 26 52 58 | 0.29 | ug: | ... | 14.212 (35) | 14.054 (43) | 14.024 (55) | ... |

TABLE 1—Continued

| Name (1) | R.A. (2000) (2) | Decl. (2000) (3) | Offset (arcsec) (4) | Type (5) | P_{orb} (days) (6) | J (mag) (7) | H (mag) (8) | K_s (mag) (9) | Notes (10) |
|----------------|-----------------------|------------------------|---------------------------|-------------|-----------------------------------|---------------------|---------------------|-----------------------|---------------|
| CW Mon | 06 36 54.5 | 00 02 16 | 1.33 | ug | 0.1762 | 13.786 (27) | 13.214 (27) | 12.944 (36) | ... |
| PU CMa | 06 40 47.7 | -24 23 15 | 0.82 | ugsu: | ... | 12.495 (30) | 12.468 (34) | 12.369 (31) | ... |
| BT Mon | 06 43 47.2 | -02 01 14 | 0.82 | na | 0.333814 | 14.397 (33) | 13.920 (41) | 13.712 (49) | ... |
| KT Gem | 06 45 21.1 | 19 04 47 | 1.67 | UGSS | ... | 16.108 (88) | > 15.797 | > 16.033 | rd200 bl100 |
| IR Gem | 06 47 34.6 | 28 06 23 | 1.30 | ugsu | 0.0684 | 15.235 (44) | 14.850 (65) | 14.534 (76) | ... |
| Mon | 06 49 50.8 | -07 37 41 | 1.23 | am | 0.183 | 15.136 (43) | 14.569 (53) | 14.287 (69) | ... |
| DN Gem | 06 54 54.4 | 32 08 27 | 0.84 | na | 0.12785 | 15.428 (57) | 15.197 (88) | 15.274 (168) | ... |
| WY CMa | 07 11 43.8 | -26 58 54 | 0.42 | cv: | ... | 14.797 (40) | 14.555 (45) | 14.461 (77) | ... |
| WZ CMa | 07 18 49.2 | -27 07 43 | 0.62 | ugz: | ... | 14.841 (39) | 14.308 (52) | 14.138 (82) | ... |
| GI Mon | 07 26 47.1 | -06 40 30 | 0.90 | na | ... | 15.344 (50) | 15.033 (74) | 14.813 (126) | ... |
| KQ Mon | 07 31 21.1 | -10 21 50 | 0.91 | ux | ... | 12.853 (34) | 12.740 (48) | 12.665 (44) | * |
| V445 Pup | 07 37 56.9 | -25 56 59 | 0.26 | n: | ... | 12.270 (31) | 11.933 (36) | 11.515 (30) | ... |
| UY Pup | 07 46 31.2 | -12 57 09 | 0.43 | ugz: | 0.423 | 14.127 (34) | 13.624 (35) | 13.495 (54) | ... |
| BV Pup | 07 49 05.3 | -23 34 01 | 0.34 | ugSS | 0.225 | 13.295 (27) | 12.886 (28) | 12.784 (34) | ... |
| Mon | 07 49 10.4 | -05 49 26 | 0.59 | am | 0.15 | 16.324 (112) | 16.146 (235) | > 15.236 | rd220 bl110 |
| PQ Gem | 07 51 17.4 | 14 44 25 | 1.23 | dq | 0.216359 | 13.401 (36) | 13.180 (40) | 12.971 (36) | * |
| HS Pup | 07 53 24.9 | -31 38 50 | 0.62 | na: | ... | 16.318 (92) | 15.856 (150) | 15.336 (172) | ... |
| BX Pup | 07 54 15.6 | -24 19 36 | 0.13 | ugz | 0.127 | 14.543 (30) | 14.048 (33) | 13.839 (56) | ... |
| U Gem | 07 55 05.3 | 22 00 06 | 1.00 | ugSS | 0.176906 | 11.625 (30) | 11.049 (37) | 10.813 (24) | * |
| DW Cnc | 07 58 53.1 | 16 16 45 | 0.60 | ug | ... | 14.662 (40) | 14.317 (54) | 14.008 (64) | ... |
| HZ Pup | 08 03 22.8 | -28 28 29 | 0.95 | na | ... | 15.886 (80) | 15.643 (132) | 15.556 (252) | ... |
| YZ Cnc | 08 10 56.6 | 28 08 34 | 0.40 | ugsu | 0.0868 | 13.143 (34) | 12.929 (34) | 12.840 (29) | ... |
| CP Pup | 08 11 46.0 | -35 21 06 | 1.36 | na | 0.06143 | 14.353 (30) | 14.205 (44) | 14.009 (66) | ... |
| VV Pup | 08 15 06.7 | -19 03 17 | 1.36 | am | 0.069747 | 15.546 (59) | 14.921 (84) | 14.526 (91) | ... |
| Z Cam | 08 25 13.2 | 73 06 39 | 0.05 | ugz | 0.289841 | 11.358 (25) | 10.810 (23) | 10.654 (30) | ... |
| AT Cnc | 08 28 36.9 | 25 20 03 | 0.38 | ugz | 0.2011 | 12.448 (29) | 12.324 (53) | 12.210 (26) | ... |
| WX Pyx | 08 33 05.7 | -22 48 32 | 1.12 | am:/dq | ... | 15.325 (51) | 14.957 (81) | 14.817 (135) | ... |
| DE Cnc | 08 35 27.3 | 19 45 30 | 1.12 | UG | ... | 16.354 (107) | 15.659 (119) | 15.673 (174) | ... |
| CC Cnc | 08 36 19.2 | 21 21 05 | 0.26 | ugsu | 0.07352 | 16.530 (128) | 16.105 (161) | 15.646 (171) | ... |
| SW UMa | 08 36 42.8 | 53 28 38 | 0.58 | ugsu/dq | 0.056815 | 15.635 (72) | 15.345 (133) | 14.772 (134) | ... |
| EI UMa | 08 38 22.0 | 48 38 02 | 0.46 | ug | 0.2681 | 13.884 (32) | 13.550 (32) | 13.545 (34) | ... |
| SY Cnc | 09 01 03.3 | 17 53 56 | 0.50 | ugz | 0.38 | 11.276 (27) | 11.037 (34) | 10.947 (33) | ... |
| GY Cnc | 09 13 50.6 | 18 49 47 | 0.40 | ug | 0.17544 | 13.949 (31) | 13.382 (35) | 13.149 (33) | ... |
| BK Lyn | 09 20 11.2 | 33 56 42 | 0.41 | nl/ug: | 0.07498 | 14.479 (42) | 14.459 (58) | 14.406 (105) | ... |
| AR Cnc | 09 22 07.5 | 31 03 15 | 1.14 | ug | 0.2146 | 16.513 (137) | 15.672 (141) | > 16.610 | rd220 bl110 |
| Leo | 09 24 56.1 | 13 20 52 | 2.58 | am | 0.169 | 13.425 (38) | 12.795 (41) | 12.509 (35) | * |
| UMa 6 | 09 32 14.9 | 49 50 54 | 1.26 | nl | 0.41838 | 15.670 (60) | 15.459 (101) | 15.274 (154) | ... |
| AG Hya | 09 50 29.8 | -23 45 18 | 1.33 | ug | ... | 15.707 (62) | 15.411 (109) | 15.075 (140) | ... |
| X Leo | 09 51 01.5 | 11 52 31 | 0.54 | ug | 0.1644 | 14.310 (28) | 13.856 (41) | 13.539 (43) | * |
| RZ LMi | 09 51 49.0 | 34 07 25 | 1.44 | ugsu | 0.0585 | 15.726 (64) | 15.693 (123) | 15.590 (163) | ... |
| Leo | 09 53 08.2 | 14 58 37 | 0.79 | am | 0.0708 | 16.249 (102) | 16.427 (264) | > 15.905 | rd220 bl110 |
| RU LMi | 10 02 07.5 | 33 51 00 | 1.20 | ug | 0.251 | 16.686 (142) | 16.442 (217) | 15.884 (270) | ... |
| UMa 7 | 10 04 34.7 | 66 29 15 | 0.74 | vy | 0.1444 | 14.747 (33) | 14.634 (50) | 14.474 (77) | ... |
| CH UMa | 10 07 00.6 | 67 32 46 | 1.40 | ug | 0.343 | 12.706 (25) | 12.167 (24) | 12.021 (26) | ... |
| SW Sex | 10 15 09.4 | -03 08 33 | 0.72 | ux | 0.134938 | 14.200 (30) | 13.993 (45) | 13.847 (61) | ... |
| RW Sex | 10 19 56.6 | -08 41 56 | 0.14 | ux | 0.24507 | 10.321 (28) | 10.143 (26) | 10.058 (26) | ... |
| LMi | 10 26 27.5 | 38 45 01 | 1.67 | am | 0.11638 | 13.431 (37) | 12.859 (33) | 12.496 (37) | * |
| Leo 5 | 10 28 00.1 | 21 48 13 | 0.41 | nl | ... | 15.602 (61) | 15.287 (92) | 15.242 (149) | ... |
| Sex | 10 39 46.9 | -05 06 58 | 0.70 | cv | ... | 16.480 (106) | 15.594 (88) | 15.380 (189) | * |
| DO Leo | 10 40 51.2 | 15 11 34 | 0.41 | nl | 0.234515 | 15.911 (73) | 15.162 (99) | 15.231 (156) | ... |
| SX LMi | 10 54 30.4 | 30 06 10 | 0.32 | ugsu | 0.0672 | 15.698 (68) | 15.545 (118) | 15.304 (162) | ... |
| Hya | 10 58 27.5 | -29 19 02 | 0.65 | ux | ... | 14.049 (36) | 13.946 (52) | 13.896 (61) | ... |
| Hya | 10 58 56.4 | -29 14 41 | 0.51 | ug: | ... | 14.479 (40) | 14.093 (51) | 13.958 (62) | ... |
| AN UMa | 11 04 25.7 | 45 03 15 | 1.26 | am | 0.079753 | 15.622 (61) | 15.481 (108) | 15.069 (110) | ... |
| ST LMi | 11 05 39.8 | 25 06 29 | 0.30 | am | 0.079089 | 14.555 (32) | 13.886 (37) | 13.401 (35) | ... |
| AR UMa | 11 15 44.7 | 42 58 22 | 0.95 | am | 0.080501 | 14.120 (38) | 13.598 (59) | 13.276 (51) | ... |
| UMa | 11 31 23.0 | 43 22 37 | 6.79 | cv | ... | 15.343 (73) | 15.170 (120) | 14.772 (160) | ... |
| Leo | 11 42 47.8 | 21 57 09 | 0.45 | cv/qso: | ... | 15.610 (79) | 14.577 (62) | 13.669 (53) | ... |
| DO Dra | 11 43 38.3 | 71 41 20 | 0.56 | dq | 0.165374 | 13.212 (27) | 12.624 (29) | 12.310 (28) | ... |
| TW Vir | 11 45 21.1 | -04 26 06 | 1.57 | ug | 0.18267 | 13.316 (23) | 13.077 (38) | 12.921 (35) | ... |
| Leo | 11 48 03.1 | 18 30 45 | 1.41 | cv | ... | 14.883 (44) | 14.914 (67) | 15.146 (118) | ... |
| EU UMa | 11 49 55.7 | 28 45 07 | 0.40 | am | 0.0626 | 16.472 (111) | 15.954 (134) | 16.050 (260) | ... |
| Crv | 11 58 34.5 | -22 33 34 | 0.06 | cv: | ... | 16.059 (86) | 15.582 (133) | > 15.399 | rd220 bl110 |
| BE CVn | 12 17 59.7 | 40 33 10 | 0.37 | ug: | ... | 16.267 (110) | 16.297 (245) | > 15.739 | rd220 bl110 |
| Dra 7 | 12 22 20.2 | 75 03 27 | 0.34 | cv | ... | 14.675 (40) | 14.592 (55) | 14.582 (95) | ... |

TABLE 1—Continued

| Name (1) | R.A. (2000) (2) | Decl. (2000) (3) | Offset (arcsec) (4) | Type (5) | P_{orb} (days) (6) | J (mag) (7) | H (mag) (8) | K_s (mag) (9) | Notes (10) |
|-----------------|-----------------------|------------------------|---------------------------|-------------|-----------------------------------|---------------------|---------------------|-----------------------|---------------------|
| CQ Dra | 12 30 06.7 | 69 12 05 | ... | cv | 0.1656 | ... | ... | ... | too bright |
| AM CVn | 12 34 54.6 | 37 37 43 | 1.21 | ibwd | 0.011907 | 14.530 (31) | 14.605 (73) | 14.442 (79) | ... |
| EX Hya | 12 52 24.4 | -29 14 57 | 2.17 | ug/dq | 0.068234 | 12.238 (25) | 11.947 (21) | 11.705 (28) | ... |
| GP Com | 13 05 42.9 | 18 01 03 | 6.11 | ibwd | 0.032339 | 15.752 (73) | 15.619 (130) | 15.154 (168) | high proper motion |
| EV UMa | 13 07 53.9 | 53 51 30 | 1.39 | am | 0.055338 | 16.343 (138) | 16.061 (229) | > 15.749 | rd220 bl110 |
| Dra 1 | 13 17 51.8 | 67 32 00 | 0.10 | cv | ... | 15.238 (49) | 14.684 (67) | 14.625 (118) | ... |
| UX UMa | 13 36 41.0 | 51 54 50 | 1.14 | ux | 0.196671 | 12.234 (24) | 11.991 (26) | 11.886 (33) | ... |
| Lib 3 | 14 50 38.7 | -24 22 50 | 0.69 | ux | ... | 14.024 (29) | 13.664 (38) | 13.756 (49) | ... |
| ES Dra | 15 25 31.8 | 62 01 00 | 0.20 | ugsu | 0.1766 | ... | 14.891 (77) | ... | ccSOS |
| HP Lib | 15 35 53.1 | -14 13 12 | 0.12 | ibwd | 0.01295 | 13.806 (25) | 13.856 (39) | 13.896 (62) | ... |
| CT Ser | 15 45 39.1 | 14 22 33 | 0.84 | n | 0.195 | 16.065 (79) | 15.600 (123) | > 15.356 | rd220 bl110 |
| QZ Ser | 15 56 55.1 | 21 07 12 | 1.41 | ug: | ... | 14.575 (32) | 14.149 (47) | 14.150 (70) | * |
| V893 Sco | 16 15 15.1 | -28 37 31 | 1.58 | ug | 0.075962 | 13.206 (29) | 12.914 (36) | 12.660 (34) | ... |
| HP Nor | 16 20 50.0 | -54 53 22 | 3.67 | ugz | ... | 14.049 (31) | 13.551 (32) | 13.307 (39) | ... |
| U Sco | 16 22 30.8 | -17 52 44 | 1.04 | nrb | 1.23056 | 16.844 (135) | 16.443 (191) | > 15.302 | rd220 bl110 |
| V841 Oph | 16 59 30.3 | -12 53 27 | 0.73 | nb | 0.60423 | 12.350 (23) | 11.963 (30) | 11.813 (28) | ... |
| V1326 Oph | 17 05 02.3 | -18 59 29 | 0.91 | UG | ... | 16.797 (152) | > 16.435 | > 15.672 | rd200 bl100 |
| FQ Sco | 17 08 04.4 | -32 42 02 | 0.84 | ugSS | ... | 13.669 (31) | 13.095 (33) | 12.762 (40) | ... |
| V2051 Oph | 17 08 19.1 | -25 48 31 | 0.87 | ugsu | 0.062428 | 14.329 (32) | 13.868 (52) | 13.515 (42) | ... |
| V795 Her | 17 12 56.1 | 33 31 21 | 2.33 | dq | 0.108247 | 12.852 (27) | 12.882 (36) | 12.780 (38) | ... |
| V825 Her | 17 18 37.0 | 41 15 51 | 0.08 | ux | 0.206 | 13.874 (34) | 13.606 (42) | 13.510 (41) | ... |
| RY Ser | 17 23 07.2 | -12 48 09 | 0.81 | ug | ... | 13.710 (36) | 13.103 (31) | 12.919 (38) | ... |
| V478 Sco | 17 25 58.5 | -35 32 31 | 0.84 | ug | ... | ... | ... | ... | ccPPP |
| V442 Oph | 17 32 15.1 | -16 15 22 | 0.54 | vy | 0.12435 | 13.331 (27) | 13.241 (29) | 13.099 (41) | ... |
| V972 Oph | 17 34 44.5 | -28 10 36 | 0.76 | nb | ... | 13.568 (30) | 12.896 (69) | 12.581 (70) | ... |
| V794 Oph | 17 38 49.3 | -22 50 48 | 0.38 | nb | ... | 14.205 (64) | 13.408 (35) | 13.226 (37) | ... |
| V733 Sco | 17 39 42.9 | -35 52 39 | 1.01 | n or m | ... | 14.579 (63) | ... | ... | cc0PP |
| V734 Sco | 17 45 02.3 | -35 38 07 | 0.88 | n or m | ... | ... | ... | ... | rd111 bl000 ccCCD * |
| Her | 17 48 05.9 | 34 04 01 | 1.11 | cv: | ... | 16.139 (89) | 15.363 (102) | 14.471 (79) | ... |
| V3964 Sgr | 17 49 42.6 | -17 23 35 | 0.88 | na | ... | 15.714 (108) | 15.371 (163) | > 14.503 | rd220 bl110 |
| V1172 Sgr | 17 50 23.5 | -20 40 30 | 1.62 | n | ... | 12.579 (28) | 11.439 (26) | 11.043 (32) | ... |
| V977 Sco | 17 51 50.1 | -32 32 01 | 0.53 | n | ... | 12.632 (38) | 11.955 (33) | 11.815 (44) | ... |
| V696 Sco | 17 53 11.5 | -35 50 15 | 1.16 | na | ... | 14.594 (52) | 14.403 (78) | 14.321 (90) | ... |
| V745 Sco | 17 55 22.1 | -33 14 57 | 2.20 | nra | ... | 10.052 (22) | 8.846 (35) | 8.233 (27) | * |
| V732 Sgr | 17 56 07.4 | -27 22 17 | 1.38 | na | ... | 13.415 (44) | 11.873 (31) | 11.197 (42) | ... |
| V1275 Sgr | 17 59 06.2 | -36 18 41 | 1.49 | na | ... | 14.287 (43) | 13.705 (45) | 13.546 (58) | ... |
| V2468 Sgr | 17 59 49.0 | -29 01 03 | 5.29 | UG: | ... | 9.182 (30) | 8.074 (41) | 7.732 (45) | rd211 bl100 * |
| EX Dra | 18 04 14.1 | 67 54 12 | 0.83 | ug | 0.209937 | 12.891 (23) | 12.269 (25) | 12.042 (27) | ... |
| DQ Her | 18 07 30.4 | 45 51 32 | 1.46 | na/dq | 0.193621 | 13.610 (25) | 13.336 (30) | 13.142 (45) | ... |
| PU Her | 18 09 52.3 | 32 00 33 | 1.28 | UG | ... | 16.350 (103) | > 16.255 | > 16.060 | rd200 bl100 |
| V533 Her | 18 14 20.5 | 41 51 23 | 0.68 | na | 0.147 | 14.694 (34) | 14.662 (51) | 14.627 (94) | ... |
| AM Her | 18 16 13.3 | 49 52 04 | 0.94 | am | 0.128927 | 12.085 (27) | 11.506 (29) | 11.149 (22) | ... |
| V4633 Sgr | 18 21 40.5 | -27 31 38 | 0.66 | na | ... | 10.542 (35) | 10.559 (31) | 9.853 (29) | ... |
| GR Sgr | 18 22 58.6 | -25 34 47 | 0.97 | n | ... | 14.846 (58) | 14.496 (88) | 14.636 (131) | * |
| V1151 Sgr | 18 25 23.7 | -20 11 59 | 1.80 | nb | ... | > 15.707 | 14.978 (84) | > 14.851 | rd020 bl010 |
| V3941 Sgr | 18 25 58.2 | -29 25 49 | 0.25 | UG: | ... | 12.049 (29) | 11.479 (25) | 11.254 (30) | ... |
| BS Sgr | 18 26 46.8 | -27 08 20 | 1.01 | nb | ... | 12.845 (31) | 12.216 (30) | 12.102 (32) | ... |
| V4362 Sgr | 18 30 23.1 | -17 11 57 | 0.09 | n | ... | 15.007 (51) | 14.581 (65) | 13.576 (49) | * |
| LL Lyr | 18 35 12.9 | 38 20 04 | 1.14 | ug | ... | 15.406 (52) | 14.879 (63) | 14.602 (85) | ... |
| BP CrA | 18 36 50.8 | -37 25 53 | 1.53 | ugz | ... | 14.023 (32) | 13.608 (38) | 13.342 (40) | ... |
| V344 Lyr | 18 44 39.2 | 43 22 27 | 0.70 | ugsu | 0.0876 | 15.618 (54) | 15.431 (99) | 15.269 (156) | ... |
| V838 Her | 18 46 31.5 | 12 14 02 | 0.19 | na | 0.297635 | 16.123 (119) | > 15.653 | 14.949 (141) | rd202 bl101 |
| V1223 Sgr | 18 55 02.2 | -31 09 48 | 1.44 | dq | 0.140244 | 12.839 (30) | 12.728 (33) | 12.640 (33) | ... |
| V493 Lyr | 19 01 31.5 | 42 54 53 | 0.26 | ug | ... | 15.664 (77) | 15.238 (104) | 14.929 (178) | ... |
| MV Lyr | 19 07 16.3 | 44 01 08 | 0.52 | vy | 0.1329 | 15.902 (83) | 15.455 (129) | 15.214 (171) | ... |
| V415 Lyr | 19 08 03.9 | 31 23 56 | 2.09 | ug: | ... | 15.793 (63) | 15.710 (137) | > 15.863 | rd220 bl110 |
| V369 Lyr | 19 11 55.0 | 32 12 07 | 0.87 | NA | ... | 16.180 (108) | > 15.840 | 15.665 (235) | rd202 bl101 * |
| Lyr | 19 17 26.5 | 37 10 41 | 0.69 | ug | ... | 15.135 (53) | 14.606 (68) | 14.468 (106) | ... |
| CZ Aql | 19 19 58.2 | -07 10 55 | 0.14 | ug | ... | 14.126 (35) | 13.786 (40) | 13.630 (49) | ... |
| V1504 Cyg | 19 28 56.5 | 43 05 37 | 0.37 | ugsu | 0.06951 | 16.139 (87) | > 15.834 | > 15.337 | rd200 bl100 |
| V868 Cyg | 19 29 04.5 | 28 54 26 | 1.52 | ugZ | ... | 15.331 (48) | 15.026 (89) | 14.949 (126) | ... |
| NQ Vul | 19 29 14.7 | 20 27 59 | 1.31 | na | ... | ... | 14.644 (62) | 14.314 (78) | rd422 bl011 |
| V1505 Cyg | 19 29 49.0 | 28 32 54 | 1.07 | UGZ | ... | 15.214 (55) | 15.100 (82) | 15.233 (160) | ... |
| V792 Cyg | 19 31 01.0 | 33 47 05 | 0.91 | ugSS | ... | 14.916 (52) | 14.407 (64) | 14.223 (75) | ... |
| KX Aql | 19 33 53.7 | 14 17 47 | 1.33 | ug | ... | 15.847 (81) | 14.834 (72) | 14.670 (103) | ... |
| Cyg 2 | 19 34 36.1 | 51 07 41 | 1.49 | ug | ... | 15.865 (67) | 15.966 (161) | 15.360 (228) | ... |
| V905 Cyg | 19 35 05.6 | 30 34 24 | 0.77 | ug | ... | 16.444 (122) | 15.832 (136) | > 15.131 | rd220 bl110 |

TABLE 1—Continued

| Name (1) | R.A. (2000) (2) | Decl. (2000) (3) | Offset (arcsec) (4) | Type (5) | P_{orb} (days) (6) | J (mag) (7) | H (mag) (8) | K_s (mag) (9) | Notes (10) |
|-----------------|-----------------------|------------------------|---------------------------|-------------|-----------------------------------|---------------------|---------------------|-----------------------|-------------------|
| EM Cyg | 19 38 40.1 | 30 30 28 | 0.45 | ugz | 0.290909 | 11.710 (27) | 11.314 (32) | 11.196 (26) | ... |
| FY Vul | 19 41 39.9 | 21 46 00 | 1.80 | ugz | ... | 13.626 (37) | 13.342 (50) | 13.200 (82) | * |
| Aql | 19 46 16.4 | -04 44 57 | 0.70 | cv | ... | 15.532 (57) | 15.097 (82) | 14.724 (109) | ... |
| V813 Cyg | 19 49 35.9 | 36 44 40 | 0.83 | ugSS | ... | ... | ... | > 15.499 | rd220 bl110 ccSS0 |
| Cyg | 19 51 47.5 | 37 16 48 | 0.39 | cv | ... | 13.252 (35) | 12.709 (33) | 12.505 (34) | ... |
| V405 Vul | 19 53 05.0 | 21 14 50 | 1.39 | ugsu | 0.113 | 14.701 (46) | 14.215 (50) | 14.154 (78) | ... |
| PQ Aql | 19 53 06.6 | 12 59 01 | 0.85 | ug: | ... | 15.991 (86) | 15.314 (94) | 15.121 (118) | ... |
| V1454 Cyg | 19 53 38.3 | 35 21 45 | 0.79 | ugSS | ... | 15.452 (59) | 15.109 (87) | 14.814 (111) | ... |
| EY Cyg | 19 54 36.8 | 32 21 55 | 0.47 | ugSS | 0.450617 | 13.081 (30) | 12.685 (36) | 12.543 (39) | ... |
| V1162 Cyg | 19 54 45.7 | 36 47 11 | 0.16 | NL: | ... | 15.571 (61) | 15.037 (72) | 14.975 (108) | ... |
| UU Aql | 19 57 18.7 | -09 19 21 | 1.32 | ug | 0.14049 | 14.268 (32) | 13.561 (39) | 13.334 (39) | ... |
| Cyg | 19 58 14.5 | 32 32 42 | 0.53 | dq | 0.1815 | 15.078 (52) | 14.774 (96) | 14.581 (105) | * |
| V4140 Sgr | 19 58 49.7 | -38 56 12 | 0.96 | ugsu: | 0.06143 | 16.649 (130) | > 16.560 | > 16.070 | rd200 bl100 |
| V823 Cyg | 20 01 49.3 | 36 07 24 | 0.56 | ugsu | ... | 15.004 (59) | 14.902 (102) | > 14.671 | rd220 bl110 * |
| V1363 Cyg | 20 06 11.6 | 33 42 38 | 0.68 | ugZ | ... | 14.259 (37) | 13.679 (64) | 13.389 (38) | ... |
| WZ Sge | 20 07 36.4 | 17 42 15 | 1.46 | ugwz/dq | 0.056688 | 14.877 (39) | 14.535 (51) | 14.019 (59) | ... |
| V1310 Cyg | 20 09 32.4 | 41 00 28 | 0.03 | ugSS | ... | 15.653 (68) | 15.177 (96) | > 14.511 | rd220 bl110 |
| V1101 Aql | 20 13 04.0 | 15 35 47 | 0.64 | ugz/cv: | 0.1442 | 14.906 (40) | 14.457 (53) | 14.426 (94) | ... |
| Cyg | 20 15 14.7 | 36 59 24 | 0.49 | cv | ... | 15.842 (121) | 14.991 (88) | > 14.910 | * |
| Cyg | 20 15 37.0 | 37 11 23 | 0.18 | cv | ... | 15.540 (78) | 15.042 (107) | 14.790 (150) | * |
| V794 Aql | 20 17 34.0 | -03 39 51 | 0.92 | vy | 0.23 | 14.177 (34) | 13.927 (40) | 13.739 (57) | ... |
| Cap 1 | 20 22 42.3 | -21 07 55 | 0.36 | cv | ... | 9.998 (25) | 9.191 (25) | 9.052 (31) | ... |
| V1776 Cyg | 20 23 30.5 | 46 31 30 | 0.06 | ux | 0.164739 | 15.255 (54) | 14.893 (86) | 14.885 (107) | ... |
| V503 Cyg | 20 27 17.4 | 43 41 23 | 0.67 | ugsu | 0.0757 | 16.359 (126) | > 15.337 | > 15.200 | rd200 bl100 * |
| V1390 Cyg | 20 28 23.4 | 39 03 54 | 1.18 | ugSU | ... | 13.549 (28) | ... | ... | cc0SS |
| AE Aqr | 20 40 09.0 | 00 52 15 | 2.13 | dq | 0.411656 | 9.486 (26) | 8.936 (24) | 8.787 (28) | ... |
| HR Del | 20 42 20.4 | 19 09 40 | 0.54 | nb | 0.214165 | 12.345 (30) | 12.293 (28) | 12.189 (26) | ... |
| V1330 Cyg | 20 52 44.8 | 35 59 27 | 0.74 | na | ... | ... | ... | ... | bl121 ccB0B |
| V1060 Cyg | 21 07 42.2 | 37 14 09 | 0.21 | UGSS | ... | 15.408 (54) | 14.686 (56) | 14.191 (86) | ... |
| HU Aqr | 21 07 58.3 | -05 17 39 | 1.68 | am | 0.08682 | 13.808 (26) | 13.500 (36) | 13.211 (40) | ... |
| V1062 Cyg | 21 08 12.0 | 36 49 29 | 2.63 | UGSS | ... | 15.597 (61) | 14.844 (62) | 14.887 (156) | ... |
| VY Aqr | 21 12 09.2 | -08 49 36 | 0.92 | ugwz | 0.06309 | 15.379 (78) | 15.025 (129) | 14.574 (124) | ... |
| V2069 Cyg | 21 23 44.8 | 42 18 02 | 0.64 | cv/dq: | 0.311683 | 14.296 (36) | 13.885 (48) | 13.712 (57) | ... |
| Cyg | 21 30 18.5 | 47 10 07 | 0.00 | cv | ... | 11.209 (26) | 10.587 (32) | 10.365 (27) | * |
| V630 Cyg | 21 34 59.2 | 40 40 18 | 0.46 | ugsu | 0.076 | 15.091 (41) | 14.948 (57) | > 14.930 | rd220 bl110 |
| Q Cyg | 21 41 43.9 | 42 50 29 | 0.12 | na | ... | 13.578 (29) | 13.259 (33) | 13.110 (37) | ... |
| SS Cyg | 21 42 42.7 | 43 35 09 | 1.57 | ugss | 0.27513 | 8.526 (9) | 8.341 (12) | 8.291 (10) | * |
| V2209 Cyg | 21 44 03.8 | 44 39 02 | 0.34 | ug: | ... | 15.144 (47) | 14.887 (82) | 14.594 (91) | ... |
| V1089 Cyg | 21 44 17.7 | 47 54 50 | 2.30 | UGSS | ... | 15.614 (67) | 14.926 (79) | 14.672 (90) | ... |
| LS Peg | 21 51 57.9 | 14 06 54 | 0.41 | dq: | 0.174774 | 11.703 (34) | 11.620 (35) | 11.493 (35) | ... |
| RU Peg | 22 14 02.6 | 12 42 11 | 0.50 | ugSS | 0.3746 | 11.059 (25) | 10.627 (35) | 10.442 (30) | ... |
| V381 Lac | 22 15 58.9 | 42 22 47 | 0.44 | nl | ... | 13.212 (24) | 10.202 (32) | 7.780 (41) | rd221 bl110 |
| FO Aqr | 22 17 55.4 | -08 21 05 | 1.06 | dq | 0.20206 | 12.886 (27) | 12.744 (33) | 12.511 (30) | ... |
| DI Lac | 22 35 48.6 | 52 43 00 | 1.05 | na | 0.543773 | 13.699 (26) | 13.519 (42) | 13.344 (40) | ... |
| V367 Peg | 22 45 00.7 | 16 55 14 | 0.62 | ug | ... | 16.411 (117) | 15.985 (165) | 15.446 (181) | ... |
| RZ Gru | 22 47 12.0 | -42 44 38 | 0.13 | ux | 0.417 | 11.964 (27) | 11.648 (36) | 11.595 (29) | ... |
| TY PsA | 22 49 39.9 | -27 06 54 | 1.29 | ugsu | 0.0841 | 14.304 (29) | 13.875 (44) | 13.623 (39) | ... |
| DK Lac | 22 49 47.0 | 53 17 20 | 1.35 | na | ... | 16.421 (154) | 15.978 (219) | > 15.725 | rd220 bl110 |
| OR And | 23 04 37.4 | 49 27 24 | 0.35 | cv/nl: | ... | 14.199 (37) | 14.132 (50) | 14.107 (65) | ... |
| Aqr 5 | 23 16 03.6 | -05 27 08 | 1.10 | am | 0.1451 | 15.225 (44) | 14.771 (63) | 14.607 (96) | ... |
| BV And | 23 27 02.1 | 50 07 13 | 0.23 | ug: | ... | 15.809 (71) | 15.344 (105) | 14.975 (116) | ... |
| HX Peg | 23 40 23.7 | 12 37 42 | 0.50 | ug/vy | 0.2008 | 13.222 (36) | 12.980 (61) | 12.900 (49) | ... |
| And | 23 44 57.5 | 43 31 22 | 0.34 | cv: | ... | 12.889 (28) | 12.722 (34) | 12.567 (35) | ... |
| VZ Scl | 23 50 09.2 | -26 22 53 | 0.73 | vy | 0.144622 | 16.101 (83) | 15.476 (126) | 15.163 (170) | ... |
| Scl | 23 50 30.5 | -31 27 34 | 1.61 | cv | ... | 15.050 (49) | 14.920 (77) | 14.551 (111) | ... |
| Peg 7 | 23 53 51.0 | 23 09 19 | 1.93 | nr/z an | ... | 11.354 (23) | 10.761 (29) | 10.507 (30) | ... |

NOTE.—Table 1 is also available in machine-readable form in the electronic edition of the *Astrophysical Journal*. Units of right ascension are hours, minutes, and seconds, and units of declination are degrees, arcminutes, and arcseconds.

If the magnetic field of the WD is nonnegligible, then the accretion disk can be truncated into an outer annulus only in the weak-field case (the intermediate polars or DQ Her stars), or disk formation can be prevented altogether in the strong field case (the polars or AM Her stars). The field

strength that differentiates these two kinds of magnetic CV is $B \sim 10$ MG. For intermediate polars, accretion proceeds in an extended curtain(s) from the inner edge of the truncated disk onto the magnetic pole(s) of the WD. For polars, matter transferred from the secondary star is entrained

directly onto the WD's field lines and channeled onto its magnetic pole(s).

The wide variety of CV types and subtypes, their properties and behavior, and observations and theory are extensively reviewed by Warner (1995).

1.2. Infrared Observation of CVs

Accretion-generated luminosity, which peaks in the optical-ultraviolet, dominates the radiated energy of most CVs. Because of this, CVs have "traditionally" been observed primarily at optical and shorter wavelengths. As a result, relatively little is known about their infrared (IR) properties. Fortunately, advances in IR detector technology during the last decade have now made this spectral region much more accessible. Investigating CVs in the IR will contribute to the understanding of properties of key system components that are expected to radiate at these wavelengths, such as the cool outer disk, the accretion stream, and (especially) the secondary star.

2. THE 2MASS DATA

The 2 Micron All-Sky Survey (2MASS) is a project to obtain J , H , and K_s images of the entire sky down to completeness limits (defined by photometry with $S/N > 10$) of $J \lesssim 15.8$, $H \lesssim 15.1$, and $K_s \lesssim 14.3$ (e.g., Skrutskie et al. 1995, 1997).² The survey detection limits are approximately 1 mag fainter in each band. Data were obtained on two identical, dedicated 1.3 m telescopes (one in each hemisphere), each utilizing a camera with three 256×256 pixel NICMOS3 (HgCdTe) arrays to enable simultaneous observation in J , H , and K_s (Stiening, Skrutskie, & Capps 1995). Array pixels are $2''$ in size, and each sky position was imaged six times for 1.3 s (giving a total exposure time on any object of 7.8 s). Spatial resolution in the images was improved via offsetting between the six subimages.

2MASS observations of the entire sky have been completed and are being processed for final release in late 2002. In the meantime, the 2MASS Second Incremental Data Release (2IDR) was made available in 2000 March. The 2IDR covers approximately 47% of the sky, and the 2IDR Point Source Catalog (PSC) contains astrometry and JHK_s photometry for 162,213,354 sources.

2.1. Target Selection and Counterpart Identification

In order to collect the near-IR photometry for all CVs located in the sky coverage of the 2IDR, we started with an input list containing 1252 targets comprising the entire contents (name, coordinates, type classification) of the "Living Edition" Catalog and Atlas of Cataclysmic Variables (Downes et al. 2001), frozen after the recent update on 2001 July 12. Using the GATOR interface,³ we searched the 2IDR PSC database in a $7''.5$ radius search circle around the coordinates of the targets in the input list. We compared near-IR source positions and images of each target field downloaded from the 2MASS database with optical CV positions and finding charts available from Downes et al. (2001), the Digitized Sky Survey, and other literature sources, in order to confirm that a near-IR source detected inside our search circle was actually the counterpart of the CV.

² We present only a brief overview of the properties of the 2MASS project; also see <http://pegasus.phast.umass.edu/> for additional information about all aspects of 2MASS.

³ See <http://irsa.ipac.caltech.edu/>.

To aid in future IR observations, Figure 1 shows K_s (in some cases J) finding charts constructed from 2MASS images for those CVs for which the appearance of the near-IR field is very different from the optical (e.g., crowded fields, significantly altered brightness ratios between field stars, field stars that have "vanished" or "materialized" in the near-IR, etc.), or for which we were unable to identify a near-IR counterpart because of crowding or source blending in the 2MASS images (see below). In some cases, the CV is not centered in the IR chart because it is located near the edge of a sky scan region (centered charts for targets located within $\lesssim 1'$ of a scan edge were constructed by combining two adjacent scan images) or of the 2MASS 2IDR sky coverage itself. Filter glint and persistence artifacts in the 2MASS images are marked with crosses. When optical finding charts were not available and the near-IR field was not crowded, we identified the near-IR counterpart based on a coordinate match only. Near-IR charts for all of these systems are shown in Figure 1, and they are noted in the Appendix. In some cases, the near-IR counterpart of the CV is too faint to be seen in the K_s image, but is visible in the J image. For these systems, we have shown the J band image in Figure 1 and labeled it with a "J" following the CV name. For CVs where we could not identify a near-IR counterpart (e.g., due to crowding of the near-IR field), the best target or position is indicated, and the chart is annotated with a question mark. In a few cases, charts are presented for CVs that were not detected in the 2MASS images (e.g., if they have potentially confusing nearby visual companions that *were* detected). These charts are annotated with an "x" following the CV name. CVs not included in Figure 1 have near-IR finding charts that are not substantially different from the optical charts given in Downes et al. (2001), were not detected by 2MASS, or are not located within the 2IDR sky coverage. Additional comments relating to the near-IR finding charts are included in the Appendix.

2.2. Number Statistics

As might be expected, approximately half of the input targets (629) lie outside of the 2IDR sky coverage. Of the remainder (623), eight are nonexistent systems (typically spurious nova detections), and 90 have been reclassified as non-CVs (typically symbiotic stars, quasars, dMe stars, etc.) after their initial discovery. Another 12% (152 targets) have accurate enough optical identification information that we could expect to identify the near-IR counterpart if it was detected, but no corresponding IR source is present in the PSC, and/or they have *no* near-IR source above the 2MASS detection limits within our $r = 7''.5$ search circle. Lack of adequate optical identification (often for classical novae in crowded fields that have faded to faint quiescent levels) excluded 95 targets. We were not able to unambiguously select the correct near-IR counterpart for 19 more targets in cases where the optical and/or near-IR field was extremely crowded (these included targets near the Galactic center and in star clusters). Eight targets have detectable and identifiable near-IR counterparts, but no photometry is available in the PSC because they lie in exclusion zones established around diffraction spikes from nearby bright stars (these might be recovered in the final 2MASS data release).

This leaves a preliminary data set of 251 CVs with near-IR counterparts that are reliably detected ($S/N \geq 10$) in the J , H , and/or K_s bands in the 2IDR PSC. Of these, the

near-IR counterparts of two CVs are saturated in the 2MASS data: CQ Dra (a CV + M giant triple; e.g., Reimers 1985) and ZZ Lep (a possible CV central star of a planetary nebula; e.g., Handler et al. 1997). Eight more have one or more bad magnitudes in J , H , and/or K_s due to source blending or confusion, or image artifacts. Finally, 29 CVs have only 95% confidence upper limit magnitudes in one or more of the near-IR bands (typically K_s). Thus, our final data set contains 212 CVs that have firmly identified near-IR counterparts with $S/N \geq 10$ photometry in all three of the J , H , and K_s bands.

The number distribution of each main CV subtype in this final data set is as follows: 33% ($n = 71$) dwarf novae, 13% ($n = 27$) nova-like CVs, 12% ($n = 25$) classical and recurrent novae, 14% ($n = 29$) magnetic CVs (12 intermediate polars and 17 polars), 1% ($n = 3$) interacting binary WD systems, and 27% ($n = 57$) uncertain/unclassified systems. We have defined each of these subtype categories to include the following classification codes given in Downes et al. (2001): dwarf novae: ug, ugz, ugss, ugsu, ugwz; nova-like CVs: nl, ux, vy; classical novae: n, na, nb, nc; recurrent novae: nr, nra, nrb; and magnetic CVs: am, dq. The uncertain/unclassified systems include the general classification code of “cv,” as well as any targets with uncertain classification (denoted with “:” or “?”) and/or conflicting classifications (e.g., “ug/vy”). In a few cases, to avoid “recounting” the same targets, we chose between multiple (but compatible) classifications. For example, DQ Her is classified “na/dq” in Downes et al. (2001), but we have considered it only as a magnetic CV (dq). WX Pyx is classified “am:/dq,” and we have again placed it in the intermediate polar (dq) group.

In the total input list of 1252 targets, 1043 are classified other than “non-cv” or “non-ex.” The overall breakdown by type is then approximately as follows: 32% dwarf novae, 6% nova-like CVs, 18% classical and recurrent novae, 9% magnetic systems (3% IPs, 6% polars), <1% interacting binary WDs, and 35% uncertain/unclassified systems. Comparison of these numbers with the statistics of our final data set shows that nova-like CVs and magnetic systems are overrepresented in the pool of reliable 2MASS detections, while uncertain/unclassified systems are underrepresented. This situation can be qualitatively explained because nova-like CVs generally have higher accretion rates, and so are overall brighter, and magnetic systems have less prominent (or no disk contribution), and so have a more prominent (unmasked) IR contribution from the secondary star. Meanwhile, many uncertain/unclassified systems are faint, and some number of these are likely spurious detections, both of which decrease the likelihood of their being detected by 2MASS.

2.3. Data Tables

The 2MASS data for CVs are presented in Tables 1–3. Table 1 gives the J , H , and K_s magnitudes for the preliminary data set (251 CVs), Table 2 lists the CVs with near-IR counterparts fainter than the 2MASS detection limits, and Table 3 gives information about the CVs whose near-IR counterpart could not be identified for various reasons. The columns of Table 1 are as follows:

Column (1).—The name of the CV as given in Downes et al. (2001). As noted in Downes et al. (2001), the convention of designating CVs that are not yet named in the

General Catalog of Variable Stars or subsequent Namelists by using the three-letter constellation abbreviation followed by a number is no longer used here. CVs that had been provisionally designated in this fashion in Downes & Shara (1993) and Downes, Webbink, & Shara (1997) maintain their designations, but new CVs are identified only by their constellations and coordinates.

Columns (2) and (3).—The right ascension and declination coordinates of the CVs. In general, these are intended primarily for target identification and ground-based telescope pointing. The more accurate and periodically updated coordinates in Downes et al. (2001) should be used if precise target positions are needed.

Column (4).—The offset, in arcseconds, between the optical position of the CV and the near-IR counterpart in the 2MASS data. The astrometric accuracy of the 2MASS PSC is better than $0''.4$

Column (5).—The CV classification type from Downes et al. (2001).

Column (6).—The orbital period, in days, from Downes et al. (2001). Orbital periods inferred from the superhump period relation of Stolz & Schoembs (1984) are listed here, but periods described by Downes et al. (2001) as “uncertain/unreliable” are not listed.

Columns (7), (8), and (9).—The J , H , and K_s magnitudes and corresponding 1σ uncertainties from the 2MASS 2IDR PSC. Magnitudes preceded by “>” are 95% confidence upper limits, and magnitudes are not given in the case of bad quality flags (see description of col. [10]). The final data set (212 CVs) can be identified as the subset from this table for which all three magnitude columns contain measured values; that is, neither J , H , nor K_s are given as upper limits, or they are not listed because of quality flags.

Column (10).—Any short notes about individual objects. An asterisk here indicates that additional information about the CV is given in the Appendix. In particular, quality flags for the 2MASS photometry are given in this column (see below).

There are three data quality flags of note: “rd_flg” (read flag, describing the photometry method), “bl_flg” (blend flag, describing the number of profiles fit during the photometry), and “cc_flg” (contamination flag, describing various photometry problems). Each flag is reported in Table 1 with a two-letter prefix signifying the flag category (rd, bl, or cc), followed by a three-digit code giving the flag values for the J , H , and K_s bands, where the first digit is the code for J , the second digit is the code for H , and so on.⁵ Acceptable values for rd_flg are 0 (source not detected, 95% confidence upper limit magnitude is given), 1 (aperture photometry magnitude), and 2 (profile-fitting magnitude); all other values indicate unusable data. Acceptable values for bl_flg are 0 (source not detected, corresponding to rd_flg = 0) and 1 (single profile fit to isolated source); values > 1 indicate multiple sources detected in a small region. Acceptable values for cc_flg are 0 (not contaminated or not detected); all other values indicate contaminated data (e.g., P, D, and S indicate different contamination artifacts

⁴ See http://www.ipac.caltech.edu/2mass/releases/second/doc/sec2_2.html#pscstrprop.

⁵ For complete descriptions of the quality flags, see <http://www.ipac.caltech.edu/2mass/releases/second/doc/explsup.html>.

TABLE 2
UNDETECTED CVs IN THE 2MASS SECOND INCREMENTAL DATA RELEASE

| Name | R.A. (2000) | Decl. (2000) | Name | R.A. (2000) | Decl. (2000) | Name | R.A. (2000) | Decl. (2000) |
|-----------------------------|----------------|-----------------|-----------------------------|----------------|-----------------|------------------------------|----------------|-----------------|
| BE Oct | 00 00 48.8 | -77 18 57 | V402 And..... | 00 11 07.3 | 30 32 36 | HP And | 00 19 09.2 | 41 27 42 |
| Tuc..... | 00 24 52.9 | -72 03 27 | EN Cet | 00 27 28.0 | -01 08 28 | LS And ^a | 00 32 10.1 | 41 58 12 |
| LT And..... | 00 35 24.3 | 39 46 17 | And | 00 38 48.0 | 41 04 38 | PT And | 00 40 24.3 | 41 04 01 |
| LL And..... | 00 41 51.5 | 26 37 21 | And | 00 42 57.6 | 41 08 12 | And | 00 49 56.0 | 43 37 45 |
| And | 00 50 01.0 | 43 33 56 | IZ And..... | 01 07 03.9 | 42 43 12 | WX Cet ^a | 01 17 04.2 | -17 56 23 |
| And | 01 31 26.1 | 36 02 39 | Hya | 01 32 42.1 | -65 54 31 | TU Tri..... | 01 39 15.3 | 31 24 19 |
| KV And | 02 17 13.8 | 40 41 31 | PQ And ^a | 02 29 29.6 | 40 02 41 | UW Tri..... | 02 45 17.3 | 33 31 26 |
| V368 Per | 02 47 32.7 | 34 58 28 | VW For..... | 02 52 51.3 | -30 37 43 | V372 Per | 02 56 40.0 | 37 08 23 |
| V400 Per ^a | 03 07 38.1 | 47 07 39 | CP Eri | 03 10 32.8 | -09 45 05 | QY Per | 03 15 36.8 | 42 28 15 |
| V336 Per | 03 22 53.9 | 41 37 02 | SV Ari | 03 25 03.3 | 19 49 53 | VX For | 03 26 46.9 | -34 26 37 |
| V701 Tau | 03 44 01.9 | 21 57 08 | Tau | 03 51 57.0 | 25 25 19 | XZ Eri ^a | 04 11 25.8 | -15 23 24 |
| Eri | 04 25 55.2 | -19 45 30 | Ori | 05 01 46.3 | -03 59 34 | XX Tau ^a | 05 19 24.5 | 16 43 00 |
| Lep..... | 06 00 33.2 | -27 09 18 | HM Gem | 06 03 09.0 | 25 14 49 | HQ Gem | 06 12 04.4 | 25 28 34 |
| CI Gem | 06 30 05.9 | 22 18 51 | UV Gem | 06 38 44.0 | 18 16 12 | DM Gem ^a | 06 44 12.1 | 29 56 42 |
| CG CMa | 07 04 05.2 | -23 45 34 | HS Cam | 07 19 14.0 | 65 57 45 | AW Gem | 07 22 41.0 | 28 30 17 |
| V496 Aur | 07 27 52.2 | 40 46 55 | Cnc ^a | 08 06 21.7 | 15 27 15 | V351 Pup..... | 08 11 38.3 | -35 07 31 |
| DY Pup ^a | 08 13 48.4 | -26 33 57 | EG Cnc | 08 43 04.0 | 27 51 50 | EU Cnc..... | 08 51 27.0 | 11 46 58 |
| Lyn | 08 54 13.9 | 39 05 37 | MM Hya | 09 14 14.0 | -06 47 45 | Lyn 2 | 09 34 23.0 | 40 38 10 |
| DV UMa ^a | 09 46 36.7 | 44 46 45 | Hya | 10 02 11.7 | -19 25 37 | CP Dra | 10 15 39.8 | 73 26 05 |
| CI UMa | 10 18 13.0 | 71 55 43 | UMa 8 | 10 23 20.2 | 44 05 09 | U Leo ^a | 10 24 03.3 | 14 00 11 |
| SS LMi | 10 34 05.4 | 31 08 08 | FH UMa | 10 47 09.9 | 63 35 14 | EL UMa..... | 10 55 07.0 | 36 59 47 |
| DP Leo..... | 11 17 16.0 | 17 57 41 | CVn 1 | 12 18 29.8 | 40 05 22 | TV Crv | 12 20 24.1 | -18 27 02 |
| FU Com | 12 30 51.5 | 27 07 10 | GT Com | 12 30 53.2 | 29 00 43 | AL Com ^a | 12 32 25.9 | 14 20 42 |
| Com | 13 08 55.0 | 29 24 25 | CT Boo | 14 08 20.9 | 53 30 40 | TT Boo | 14 57 44.7 | 40 43 42 |
| NY Ser | 15 13 02.3 | 23 15 08 | DM Dra ^a | 15 34 12.1 | 59 48 32 | VW CrB | 16 00 04.0 | 33 11 15 |
| V844 Her | 16 25 01.7 | 39 09 27 | V610 Her | 16 43 39.2 | 22 31 26 | V840 Oph | 16 54 44.0 | -29 37 26 |
| V2214 Oph..... | 17 12 01.6 | -29 37 33 | V1007 Her | 17 24 06.3 | 41 14 09 | V2109 Oph | 17 24 15.9 | -24 36 50 |
| BB Oph | 17 24 30.0 | -24 48 06 | V719 Sco | 17 45 43.7 | -34 00 55 | V825 Sco | 17 49 53.7 | -33 32 14 |
| V697 Sco | 17 51 21.8 | -37 24 55 | V4092 Sgr | 17 53 42.0 | -29 02 08 | V1141 Sco | 17 54 11.2 | -30 02 52 |
| V4642 Sgr | 17 55 09.8 | -19 46 01 | V1142 Sco | 17 55 25.0 | -31 01 41 | V3889 Sgr ^a | 17 58 21.3 | -28 21 53 |
| V4135 Sgr | 17 59 45.1 | -32 16 21 | V394 CrA ^a | 18 00 26.0 | -39 00 35 | V551 Sgr..... | 18 00 56.2 | -34 35 42 |
| V384 Sco | 18 01 43.2 | -35 39 28 | V1008 Her | 18 05 46.0 | 31 40 18 | V737 Sgr..... | 18 07 08.7 | -28 44 52 |
| PR Her | 18 08 04.5 | 38 46 16 | V630 Sgr | 18 08 48.3 | -34 20 21 | DV Dra ^a | 18 17 23.1 | 50 48 18 |
| V632 Her | 18 19 41.0 | 24 33 14 | V4361 Sgr | 18 23 42.5 | -18 07 15 | V909 Sgr..... | 18 25 52.3 | -35 01 27 |
| HS Sgr | 18 28 03.4 | -21 34 25 | V394 Lyr | 18 28 47.0 | 35 49 29 | FV Sct ^a | 18 34 51.6 | -12 55 27 |
| Her..... | 18 35 56.3 | 22 26 40 | V4021 Sgr | 18 38 14.0 | -23 22 47 | V693 CrA..... | 18 41 57.8 | -37 31 14 |
| DM Lyr | 18 58 44.5 | 30 15 33 | V358 Lyr | 18 59 34.0 | 42 24 10 | V447 Lyr | 19 00 19.9 | 44 27 45 |
| V1425 Aql..... | 19 05 26.6 | -01 42 03 | V1493 Aql | 19 07 36.9 | 12 31 27 | V363 Lyr | 19 08 51.6 | 43 00 32 |
| V452 Lyr | 19 10 26.3 | 43 28 55 | Lyr | 19 13 58.4 | 40 44 12 | V516 Lyr | 19 20 35.7 | 37 44 53 |
| V523 Lyr | 19 21 07.4 | 37 47 57 | WY Sge ^a | 19 32 43.8 | 17 44 55 | V793 Cyg..... | 19 33 06.2 | 33 15 37 |
| EY Aql | 19 34 44.5 | 15 01 52 | V1153 Cyg..... | 19 48 15.0 | 34 52 02 | V1449 Cyg | 19 49 16.6 | 34 10 49 |
| DO Vul | 19 52 11.0 | 19 34 42 | V465 Cyg ^a | 19 52 37.8 | 36 33 53 | V1819 Cyg ^a | 19 54 37.6 | 35 42 17 |
| AW Sge | 19 58 37.1 | 16 41 29 | V1028 Cyg..... | 20 00 56.6 | 56 56 37 | V1032 Cyg | 20 02 40.1 | 57 16 26 |
| V550 Cyg | 20 05 05.3 | 32 21 22 | AX Cap | 20 08 56.9 | -17 16 38 | ET Sge..... | 20 09 06.3 | 17 43 38 |
| V1316 Cyg | 20 12 13.6 | 42 45 51 | Cyg ^a | 20 15 36.0 | 37 04 57 | V4738 Sgr | 20 22 37.5 | -39 54 13 |
| V450 Cyg ^a | 20 58 47.4 | 35 56 28 | V1065 Cyg..... | 21 10 59.1 | 38 57 13 | V1075 Cyg | 21 29 18.8 | 42 19 12 |
| Cap 3 | 21 34 06.1 | -18 51 46 | Cap 2 | 21 39 58.5 | -23 11 44 | V1668 Cyg ^a | 21 42 35.2 | 44 01 55 |
| II Aqr..... | 22 16 27.5 | -20 27 25 | MN Lac | 22 23 04.0 | 52 41 00 | MR Lac | 22 24 42.9 | 50 31 41 |
| Aqr 3 | 22 43 31.9 | 00 12 33 | V369 Peg | 23 03 42.0 | 17 17 56 | OS And ^a | 23 12 06.0 | 47 28 20 |
| EG Aqr ^a | 23 25 19.2 | -08 18 19 | EH Aqr | 23 34 05.7 | -22 48 39 | Peg | 23 38 48.7 | 28 19 55 |
| Aqr..... | 23 49 42.3 | -09 08 03 | And 2 | 23 50 16.9 | 46 59 22 | | | |

NOTE.—Table 2 is also available in machine-readable form in the electronic edition of the *Astrophysical Journal*. Units of right ascension are hours, minutes, and seconds, and units of declination are degrees, arcminutes, and arcseconds.

^a Additional comment available; see the Appendix.

caused by a nearby bright star, C indicates confusion with a nearby source, and B indicates confusion during merging of the J -, H -, and K_s -band data sets). A CV with optimum photometry has flag values of “rd222 bl111 cc000,” and this is the case unless otherwise noted in column (10) of Table 1.

The contents of the columns in Tables 2 and 3 are the same as the correspondingly named columns of Table 1.

The Notes column in Table 3, however, contains different annotations than in Table 1, as follows:

Uncertain ID.—A CV for which there is insufficient or imprecise information pertaining to its optical position and/or identification that precludes identification of the near-IR counterpart.

TABLE 3
 PROBLEMATIC CVs IN THE 2MASS SECOND INCREMENTAL DATA RELEASE

| Name | R.A. (2000) | Decl. (2000) | Notes | Name | R.A. (2000) | Decl. (2000) | Notes |
|----------------|----------------|-----------------|------------------|----------------|----------------|-----------------|------------------|
| Tuc..... | 00 01 54.9 | -67 07 47 | uncertain ID | Cas..... | 00 12 42.0 | 52 47 24 | uncertain ID |
| Tuc 1..... | 00 24 04.3 | -72 04 58 | cluster NGC 104 | Tuc..... | 00 24 05.0 | -72 04 55 | cluster NGC 104 |
| Tuc..... | 00 24 05.2 | -72 04 51 | cluster NGC 104 | Tuc..... | 00 24 06.0 | -72 04 56 | cluster NGC 104 |
| Tuc..... | 00 24 06.5 | -72 04 43 | cluster NGC 104 | Tuc..... | 00 24 10.0 | -72 04 52 | cluster NGC 104 |
| And..... | 00 32 23.1 | 25 48 21 | uncertain ID | VZ Tuc..... | 00 34 01.0 | -73 16 16 | uncertain ID |
| And..... | 00 37 50.3 | 41 21 12 | uncertain ID | And..... | 00 41 40.9 | 41 03 37 | uncertain ID |
| And..... | 01 27 50.6 | 38 08 12 | uncertain ID | AS Psc..... | 01 28 09.0 | 31 15 03 | uncertain ID |
| Per..... | 02 29 37.1 | 52 25 40 | uncertain ID | Ari..... | 02 44 57.0 | 27 31 14 | uncertain ID |
| SU Ari..... | 02 48 30.0 | 17 21 47 | uncertain ID | Eri..... | 03 11 20.0 | -22 54 38 | uncertain ID |
| Per..... | 03 19 06.8 | 35 29 36 | uncertain ID | W Ari..... | 03 20 45.1 | 28 57 14 | uncertain ID |
| SZ Per..... | 03 47 06.3 | 34 19 18 | uncertain ID | RY Dor..... | 05 14 58.0 | -66 50 12 | uncertain ID |
| FS Aur..... | 05 47 48.3 | 28 35 11 | artifact | SS Aur..... | 06 13 22.4 | 47 44 26 | artifact * |
| SY Gem..... | 06 40 37.0 | 31 11 26 | uncertain ID | CMa..... | 06 43 58.9 | -20 52 33 | uncertain ID |
| Gem..... | 06 58 45.0 | 17 02 11 | uncertain ID | EU CMa..... | 07 05 41.0 | -16 08 47 | uncertain ID |
| VZ Gem..... | 08 07 47.0 | 30 50 54 | uncertain ID | Lyn..... | 09 06 19.2 | 44 58 47 | uncertain ID |
| HH Cnc..... | 09 16 50.7 | 28 49 42 | uncertain ID | Leo..... | 09 28 45.0 | 23 11 00 | uncertain ID |
| Leo..... | 09 37 19.0 | 15 13 12 | uncertain ID | CE UMa..... | 11 16 11.0 | 29 21 37 | uncertain ID |
| UMa..... | 11 58 32.1 | 43 56 54 | uncertain ID | FY Com..... | 12 49 16.0 | 27 25 22 | uncertain ID |
| Cen..... | 13 26 52.1 | -47 29 36 | cluster NGC 5139 | Cen..... | 13 26 53.5 | -47 29 01 | cluster NGC 5139 |
| DR UMa..... | 13 59 05.4 | 55 44 04 | uncertain ID | AB Boo..... | 14 07 04.4 | 20 44 45 | uncertain ID |
| T Boo..... | 14 14 05.7 | 19 04 02 | uncertain ID | Dra..... | 16 31 25.9 | 73 54 11 | uncertain ID |
| Her..... | 16 41 43.7 | 36 28 05 | cluster NGC 6205 | Her..... | 16 41 45.1 | 36 27 39 | cluster NGC 6205 |
| V1548 Oph..... | 17 11 26.0 | -16 20 19 | uncertain ID | V2400 Oph..... | 17 12 36.5 | -24 14 45 | artifact |
| V2264 Oph..... | 17 20 20.8 | -26 46 26 | uncertain ID | V729 Sco..... | 17 22 02.7 | -32 05 49 | uncertain ID |
| V906 Oph..... | 17 26 00.7 | -21 54 28 | uncertain ID | V908 Oph..... | 17 27 51.0 | -27 45 00 | uncertain ID |
| V2487 Oph..... | 17 31 59.8 | -19 13 56 | uncertain ID | V2313 Oph..... | 17 35 44.6 | -19 19 34 | uncertain ID |
| V1012 Oph..... | 17 41 34.4 | -23 23 33 | uncertain ID | V2024 Oph..... | 17 42 21.0 | -24 59 00 | uncertain ID |
| V721 Sco..... | 17 42 28.9 | -34 40 42 | uncertain ID | V553 Oph..... | 17 42 53.5 | -24 51 26 | uncertain ID |
| V2290 Oph..... | 17 43 05.5 | -20 07 00 | uncertain ID | KP Sco..... | 17 44 16.5 | -35 43 24 | uncertain ID |
| Sco..... | 17 47 38.0 | -33 11 55 | uncertain ID | V707 Sco..... | 17 48 26.4 | -36 37 55 | uncertain ID |
| V722 Sco..... | 17 48 37.0 | -34 57 50 | uncertain ID | V3888 Sgr..... | 17 48 40.5 | -18 45 37 | artifact |
| V1274 Sgr..... | 17 48 55.0 | -17 51 55 | uncertain ID | Sgr..... | 17 49 11.0 | -17 50 49 | uncertain ID |
| V723 Sco..... | 17 50 05.2 | -35 23 58 | uncertain ID | V759 Sgr..... | 17 50 19.7 | -27 25 02 | crowded * |
| V720 Sco..... | 17 51 58.0 | -35 23 22 | uncertain ID | V2415 Sgr..... | 17 53 12.0 | -29 34 25 | uncertain ID |
| V744 Sco..... | 17 53 18.1 | -31 13 35 | uncertain ID | Sco..... | 17 53 40.0 | -30 45 32 | uncertain ID |
| V711 Sco..... | 17 54 06.0 | -34 21 16 | uncertain ID | V4643 Sgr..... | 17 54 40.5 | -26 14 15 | uncertain ID |
| Sgr..... | 17 54 43.0 | -28 41 41 | uncertain ID | V960 Sco..... | 17 56 34.1 | -31 49 36 | uncertain ID |
| V1178 Sco..... | 17 57 07.0 | -32 23 05 | uncertain ID | V990 Sgr..... | 17 57 19.0 | -28 19 07 | crowded * |
| V787 Sgr..... | 18 00 02.2 | -30 30 31 | uncertain ID | FL Sgr..... | 18 00 30.2 | -34 36 13 | uncertain ID |
| V1014 Sgr..... | 18 06 45.7 | -27 26 15 | uncertain ID | V927 Sgr..... | 18 07 42.7 | -33 21 17 | uncertain ID |
| V617 Sgr..... | 18 07 50.8 | -35 10 25 | artifact | V631 Her..... | 18 08 44.0 | 34 27 34 | uncertain ID |
| V1015 Sgr..... | 18 09 03.0 | -32 28 16 | uncertain ID | V4160 Sgr..... | 18 14 13.8 | -32 12 28 | uncertain ID |
| V1010 Her..... | 18 14 14.3 | 30 43 37 | uncertain ID | V1175 Sgr..... | 18 14 17.0 | -31 07 08 | uncertain ID |
| V4074 Sgr..... | 18 16 05.3 | -30 51 15 | blended * | V2839 Sgr..... | 18 16 19.0 | -31 42 14 | uncertain ID |
| V4049 Sgr..... | 18 20 38.1 | -27 56 26 | uncertain ID | V441 Sgr..... | 18 22 08.1 | -25 28 54 | uncertain ID |
| V4169 Sgr..... | 18 23 26.9 | -28 22 00 | uncertain ID | Sgr..... | 18 23 40.8 | -30 21 35 | cluster NGC 6624 |
| V4171 Sgr..... | 18 23 41.3 | -22 59 29 | uncertain ID | Sgr..... | 18 23 41.4 | -30 21 57 | cluster NGC 6624 |
| V366 Sct..... | 18 29 42.8 | -12 18 55 | uncertain ID | Sgr 2..... | 18 31 23.5 | -32 20 49 | cluster NGC 6637 |
| V2359 Sgr..... | 18 31 35.0 | -32 25 52 | uncertain ID | V2572 Sgr..... | 18 31 36.7 | -32 35 58 | uncertain ID |
| V463 Sct..... | 18 34 03.2 | -14 45 11 | uncertain ID | V662 CrA..... | 18 35 31.0 | -36 56 51 | uncertain ID |
| V3645 Sgr..... | 18 35 49.2 | -18 41 45 | uncertain ID | Lyr..... | 18 53 10.0 | 35 47 00 | uncertain ID |
| V446 Her..... | 18 57 21.6 | 13 14 29 | blended * | Aql..... | 19 01 59.5 | 13 52 30 | uncertain ID |
| Aql..... | 19 02 56.7 | 15 09 41 | uncertain ID | Aql..... | 19 05 36.7 | 14 11 48 | uncertain ID |
| Aql 3..... | 19 15 54.7 | 00 14 43 | uncertain ID | V1114 Cyg..... | 19 24 36.4 | 28 26 11 | uncertain ID * |
| PW Vul..... | 19 26 05.0 | 27 21 58 | blended * | V795 Cyg..... | 19 34 34.1 | 31 32 13 | uncertain ID |
| Sgr 1..... | 19 43 57.0 | -40 26 00 | uncertain ID | V811 Cyg..... | 19 48 23.3 | 36 26 23 | artifact |
| V1452 Cyg..... | 19 52 02.0 | 35 55 34 | uncertain ID | V337 Cyg..... | 19 59 54.0 | 39 13 58 | uncertain ID |
| V1377 Cyg..... | 20 16 49.0 | 38 21 08 | uncertain ID | Cap..... | 20 24 59.4 | -22 33 22 | uncertain ID |
| V1697 Cyg..... | 20 43 17.0 | 42 42 39 | uncertain ID | CV Aqr..... | 21 21 46.0 | -14 17 39 | uncertain ID |

NOTE.—Table 3 is also available in machine-readable form in the electronic edition of the *Astrophysical Journal*. Units of right ascension are hours, minutes, and seconds, and units of declination are degrees, arcminutes, and arcseconds.

Cluster.—A CV located in a star cluster that is too crowded to obtain 2MASS photometry. The cluster’s NGC catalog number is given.

Artifact.—A CV located in the exclusion region defined around diffraction spikes of nearby bright stars.

Crowded.—The near-IR field around the CV is more crowded than the optical field, and conclusive identification of the CV’s near-IR counterpart is not possible.

Blended.—The near-IR counterpart of the CV is blended with one or more additional near-IR sources in the 2MASS images.

2.4. Comparison of 2MASS and Literature Photometry

We compiled the available near-IR magnitudes of CVs from various literature sources (e.g., Szkody & Capps 1980; Sherrington & Jameson 1983; Szkody 1987; Harrison 1992; Weight et al. 1994; Sproats, Howell, & Mason 1996). This resulted in 62 CVs with both 2MASS and literature J magnitudes, 46 with H , and 55 with K . These data are shown in Figure 2. Because it was not possible in some cases to determine the photometric system used for the literature magnitudes, and transformation relations to the 2MASS system do not exist for some of the photometric systems that were used, we have not attempted to convert the literature magnitudes to the 2MASS system. While this will inevitably increase the scatter in the relation between the 2MASS and

literature data, the transformation relations derived by Carpenter (2001) between 2MASS and numerous other photometric systems suggests that this effect will be at the less than 10% level. The intrinsic variability of the CVs during the typically long intervals (years) between the times of observation of the 2MASS and various literature magnitudes is more likely to dominate the scatter in the data.

The means and 1σ rms scatters of the Δmag values shown in Figure 2 are $\langle\Delta J\rangle = 0.015$ mag, $\langle\Delta H\rangle = -0.011$ mag, and $\langle\Delta K\rangle = -0.014$ mag, with $\sigma_{\Delta J} = 0.734$ mag, $\sigma_{\Delta H} = 0.565$ mag, and $\sigma_{\Delta K} = 0.655$ mag. If we ignore points outside the range $\Delta\text{mag} = \pm 0.75$ (shown as the dotted lines in the bottom panels of Fig. 2), then these values change to $\langle\Delta J\rangle = -0.018$ mag, $\langle\Delta H\rangle = -0.025$ mag, and $\langle\Delta K\rangle = -0.044$ mag, with $\sigma_{\Delta J} = 0.255$ mag, $\sigma_{\Delta H} = 0.256$ mag, and $\sigma_{\Delta K} = 0.226$ mag. This data range boundary was (arbitrarily) chosen to exclude only the outlying Δmag points (which likely correspond to measurements obtained during different photometric states; e.g., eclipse vs. out of eclipse, “high” vs. “low” accretion, etc.), while keeping the majority of the points that display a tendency to cluster around $\Delta\text{mag} = 0$. These results suggest that, regardless of photometric system (or, rather, on average over numerous photometric systems), the 2MASS magnitudes are slightly brighter than those measured in other photometric systems. The scatter values of ≈ 0.25 mag in all three near-IR bands

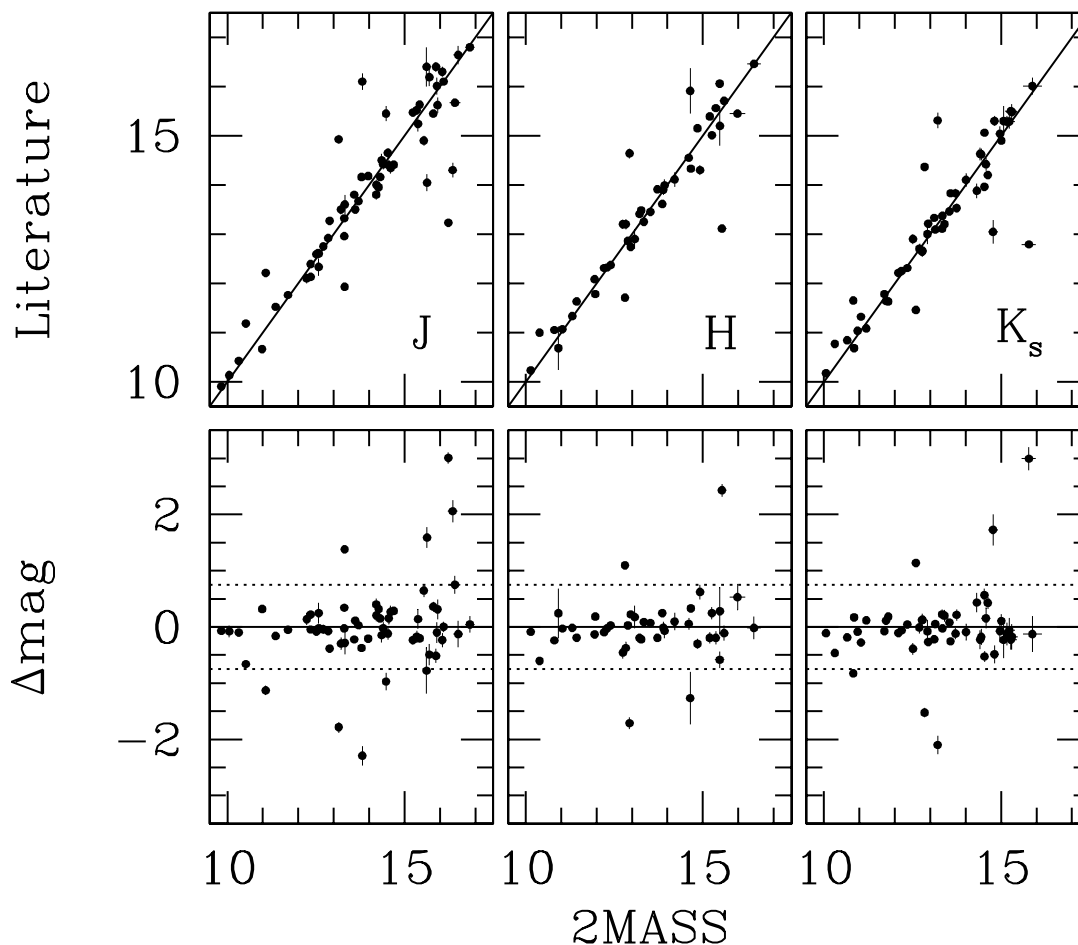


FIG. 2.—Comparison of 2MASS and literature magnitudes of CVs. The top row is a direct comparison of the data; the solid line is *not* a fit, but the line of 1:1 correspondence. The bottom row illustrates the differences in the magnitudes, $\Delta\text{mag} = (2\text{MASS} - \text{literature})$; the solid lines show $\Delta\text{mag} = 0$, while the dotted lines delimit an (arbitrary) range of $\Delta\text{mag} = \pm 0.75$.

are consistent with the combination of two 0.10–0.15 mag components corresponding to differences between photometric systems plus intrinsic near-IR variability of the CVs.

2.5. Photometric Uncertainties

Figure 3 shows the 1σ uncertainties of all CV magnitudes measured by 2MASS, as a function of the magnitude in each of the three corresponding near-IR bands. The uncertainties are generally smaller than 0.05 mag out to limiting brightnesses of $J \approx 15$, $H \approx 14$, and $K_s \approx 13.5$. The uncertainties reach maximum values of 0.26–0.28 mag at the detection limits of the PSC. In the subsequent analysis in this paper, we have not included error bars in the color-color diagrams for the sake of clarity, but have indicated whether the uncertainties are larger or smaller than 0.1 mag by using small and large data points, respectively. (Of course, given a specific target, the exact uncertainties of its color indices can be calculated directly from the information in Table 1.)

3. ANALYSIS

3.1. Color-Color Diagrams

As the first step in analyzing the IR properties of CVs from the 2MASS data, we have plotted the near-IR magnitudes of our final data set as color-color diagrams differentiated by CV classification type. These are shown in Figures 4–8 and described below. All of the figures are plotted on the same scale to facilitate comparison. The axis ranges were chosen to optimize clarity of the figures; this resulted in the omission of five CVs with $(H - K_s) > +1.05$ and/or $(J - H) > +1.30$. Each of the omitted systems is discussed in the appropriate section below. Fiducial near-IR colors of main-sequence and giant stars are shown for comparison, and described in the caption to Figure 4. In addition, the approximate region occupied by isolated WDs in the near-IR color-color diagram (Leggett 1989) is enclosed with

a dashed line.⁶ We note here that in all of the color-color diagrams, we have provided a dereddening vector, but have not applied a dereddening correction to the data. This is primarily because of the lack of known or accurate reddening values for many of the CVs in our sample. In any case, reddenings of CVs are typically small to negligible, even more so in the IR. The only instance in which we expect that this axiom might be violated is for the classical novae, some of which are believed to lie at significant distances (≥ 1 kpc). However, inspection of the color-color diagram for classical novae (see § 3.1.4) does not suggest any strong bias due to uncorrected reddening.

3.1.1. The Dwarf Novae

Figure 4 shows the data for dwarf novae (DNe). The points in Figure 4 are symbol-coded according to the optical brightness state of each DN at the time of its 2MASS observation, compiled from the American Association of Variable Star Observers (AAVSO) and Variable Star Network (VSNET) Web sites.⁷ All but 2 of the 13 systems known to have been in outburst, or on the rise to or decline from outburst, during their 2MASS observation are systematically bluer than the other systems. This is not unexpected, since the outburst state of DNe is characterized by enhanced accretion and higher accretion-generated luminosity. A handful of additional DNe with no available brightness state information also populate this region of the color-color diagram, and may have been in outburst at the times of their observations by 2MASS.

One of the hoped-for goals of observing CVs in the IR is to isolate the luminosity contribution of the secondary

⁶ Green, Ali, & Napiwotzki (2000) and Bergeron, Leggett, & Ruiz (2001) have obtained more contemporary IR observations of WDs; however, the former lack H -band data, and the latter deal with only cool ($T \lesssim 12,000$ K) WDs. We are currently preparing a report on the IR properties of all WDs detected by 2MASS.

⁷ See <http://www.aavso.org/> and <http://www.kusastro.kyoto-u.ac.jp/vsnet/>, respectively.

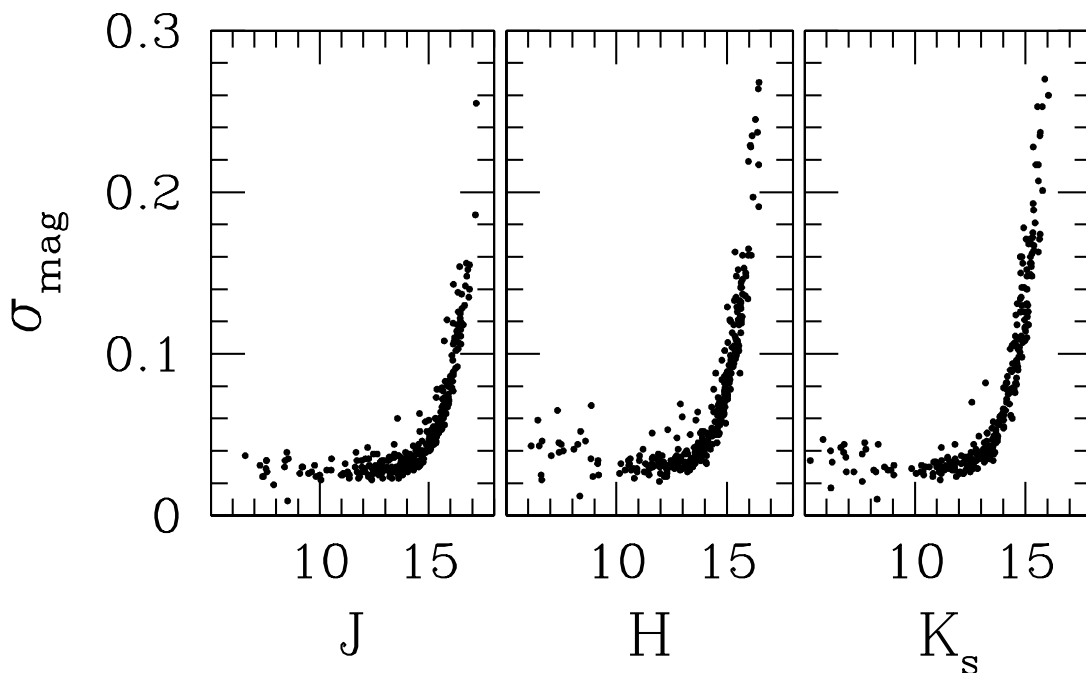


FIG. 3.—Photometric uncertainties as a function of magnitude for CVs in the 2MASS 2IDR PSC

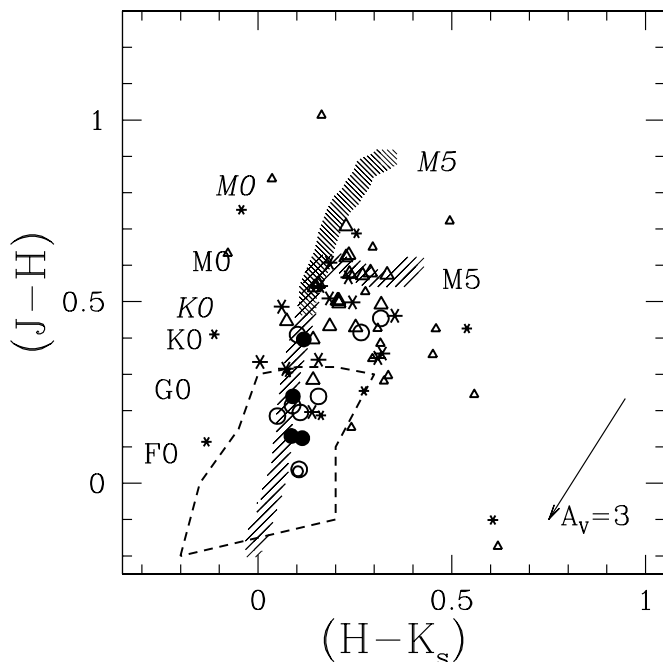


FIG. 4.—IR color-color diagram for dwarf novae. The lighter cross-hatched area shows the near-IR colors of the main sequence (Cox 2000, pp. 151–2) transformed to the 2MASS photometric system using the relations in Carpenter (2001). Positions of spectral types ranging from F0 to M5 are labeled in roman font, at the corresponding $J-H$ value but offset in $H-K_s$. Similarly, the more densely cross-hatched area shows the near-IR colors of the giant branch (luminosity class III), with spectral types from K0 to M5 labeled in italic font. The approximate region occupied by WDs (Leggett 1989) is enclosed with a dashed line. A dereddening vector corresponding to $A_V = 3$ is shown. The points are symbol-coded according to the optical brightness state of each dwarf nova at the time of its 2MASS observation (see text): *asterisks*: optical brightness information not available; *open triangles*: quiescent; *open circles*: on the rise to or decline from outburst; *filled circles*: outburst. In addition, large points have 1σ uncertainties of ≤ 0.1 mag, while small points have 1σ uncertainties of > 0.1 mag.

stars, and to learn more about the mass donors in these systems. It is potentially misleading that the near-IR colors of DNe in outburst appear very similar to F–K main-sequence stars. As is shown in § 3.3, in most CVs there is still a substantial and systematic contamination of the near-IR luminosity by the accretion process. Thus, while the apparent agreement of IR colors of DNe in outburst with those of F–K stars should not be assumed to imply anything about the nature of the secondary stars themselves, it can perhaps suggest that characteristic temperatures and emissive properties of CV accretion disks in outburst are comparable to F–K photospheres. (Most of the DNe in outburst also lie in the region of WD colors, but we expect that the accretion disk dominates over the WD during DNe outbursts. It is an unfortunate coincidence that the near-IR colors of isolated WDs are so similar to those of main-sequence stars with spectral types earlier than K.)

In contrast, many of the quiescent DNe have near-IR colors that place them along the lower main sequence. Comparison with the diskless polars (see § 3.1.3 and Fig. 6) suggests that these CVs may actually have little or, in extreme cases, no luminosity contribution from the accretion process masking their secondary stars. This is strong evidence that the accretion rate (although not necessarily the mass-transfer rate) in quiescent DNe can be very small.

Six points in Figure 4 form a weak sequence parallel to the giant track at a blue offset of $\Delta(H-K_s) \approx -0.2$. Three of these systems were known to be in their quiescent state; no brightness information was available for the other three. The colors of all of these CVs have 1σ uncertainties larger than 0.1 mag; however, their offset from the main-sequence/giant track is still significant and cannot be accounted for solely by the photometric uncertainties. The position of the blue sequence in the color-color diagram could be explained if these CVs are systematically brighter in H than the other DNe. A number of spectral lines are located in the H band, including several high-order Brackett H lines, as well as lines of He I, He II, and Fe II. If any of these lines are strongly in emission, then the H magnitude for affected systems would be brighter than in CVs without strong emission. This would require that associated lines in the K_s band (e.g., Br γ) are not also strongly in emission. Available K -band spectra of CVs (e.g., Ramseyer et al. 1993; Dhillon et al. 2000) typically show strong Br γ emission, so it is not likely that strong Brackett series emission in the H band is the culprit. An alternative explanation is that there is a strong H -band continuum source in these CVs, although its possible origin (a local maximum in the accretion disk spectral energy distribution? An optically thick bright spot at the accretion stream impact site? etc.) is uncertain.

Seven of the DNe have $(H-K_s) \gtrsim +0.4$, which sets them apart redward from the bulk of the data. These CVs also have large uncertainties on their 2MASS magnitudes. Unlike the blue offset systems discussed above, it is possible that most of these are simply large σ deviations from the region in the color-color diagram occupied by the bulk of the DNe. With the exception of the two points with $(J-H) < 0.0$ (Cyg 2 and FO And, whose locations in the color-color diagram defy a simple explanation), it is also possible that these systems may be affected by some interstellar or intrinsic reddening.

3.1.2. The Nova-like CVs

Figure 5 shows the data for nova-like CVs (NLs). Almost all of the NLs cluster in the color-color diagram in a region bounded by $-0.1 \lesssim (H-K_s) \lesssim +0.3$ and $+0.1 \lesssim (J-H) \lesssim +0.4$. This is the blue corner of the diagram, consistent with the expectation that NLs have high mass transfer and accretion rates, and prominent disks. It is also somewhat misleading, since (as with the DNe in outburst) it shows that NLs have near-IR colors similar to F–K main-sequence stars. (Again, as with the DNe in outburst, we do not expect that the near-IR colors of the NLs are dominated by their WDs.) While it is true that, in general, the secondary stars in NLs should have earlier spectral types, because of their dominance of the orbital period regime above the 2–3 hr “period gap” (e.g., Shafter 1992), we do not expect that this is providing accurate information about the spectral types of the secondary stars in NLs (see § 3.3).

The two data points shown as open circles in Figure 5 are KR Aur at $(H-K_s) \approx -0.25$ (Shafter 1983) and MV Lyr at $(H-K_s) \approx +0.25$ (Szkody & Downes 1982). Both of these NLs were in faint states during their 2MASS observation, according to data on the AAVSO and VSNET Web sites, respectively. By extension, the other two outlying NLs (i.e., with $J-H > +0.5$) in this diagram may also have been in faint states during the 2MASS observations (no optical brightness information is available for these systems). Like

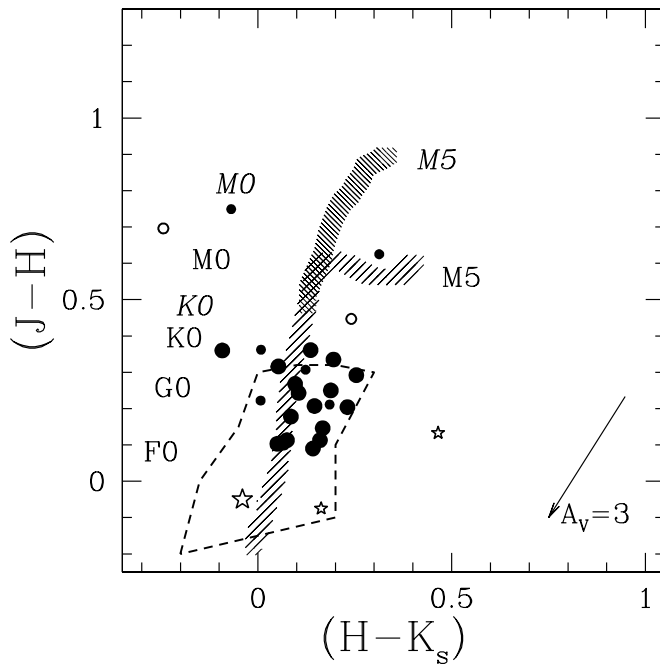


FIG. 5.—IR color-color diagram for nova-like CVs, as described in the caption to Fig. 4. The two open circles are discussed in the text. The three star-shaped points are interacting binary white dwarf systems; from low to high $(H - K_s)$ they are HP Lib, AM CVn, and GP Com.

KR Aur and MV Lyr, at least one of the other two, VZ Scl (with $H - K_s \approx +0.3$ and $J - H \approx +0.6$; O’Donoghue, Fairall, & Warner 1987), is known to be one of a subtype of NL called an “anti-dwarf nova” or VY Scl star, that occasionally drops to a faint state for several weeks at a time. The near-IR magnitudes of VZ Scl from 2MASS (see Table 1) are very similar to those obtained during another faint state of the CV in 1982: $J = 16.10$ (4), $H = 16.06$ (8), and $K = 15.29$ (11) (Sherrington, Jameson, & Bailey 1984). The other outlying system is DO Leo, an otherwise unremarkable eclipsing CV (Abbott et al. 1990). DO Leo is currently unclassified other than “nova-like” and may be another VY Scl star. One NL system, V381 Lac (Dahmark 1996), is not visible within the axis ranges of Figure 5. Its colors are extremely red, $(H - K_s) \approx +2.4$ and $(J - H) \approx +3.0$. V381 Lac is little-studied, and it could be heavily reddened and/or a misclassified symbiotic star.

The three points depicted as stars in Figure 5 are the interacting binary white dwarf systems AM CVn, GP Com, and HP Lib. In these double-degenerate CVs, the WD primary star is accreting from a mass donor that is also a WD, typically a helium WD (see review in Warner 1995, pp. 489–501). As might be expected, these systems are quite blue and lie within the WD region in the diagram, with the exception of GP Com, which may be reddened. Since GP Com is a high proper motion system thought to be relatively nearby (distance less than 100 pc; Marsh 1999), any substantial reddening would have to be intrinsic to the binary. Dhillon et al. (2000) found that the K -band spectrum of GP Com is dominated by the accretion disk and is fitted well by a model consisting of an $\sim 11,000$ K optically thin “slab.” If the disk dominates the IR luminosity of GP Com, then it may suffer from intrinsic reddening by disk material.

3.1.3. The Magnetic CVs

Figure 6 shows the data for magnetic CVs. There is a fairly sharp delineation between the near-IR colors of the strongly magnetic polars and weakly magnetic intermediate polars (IPs). Many of the polars have colors consistent with late main-sequence stars (M0–M5+). Because of the lack of an accretion disk in these systems, they are the one class in which we expect the near-IR colors of CVs to deviate little or not at all from those of the underlying secondary stars. Many of the IPs are located in the WD region. While it is possible that the WDs in these systems are more visible owing to their truncated disks, we do not believe that the WDs are actually driving the observed near-IR colors of the IPs. We would then expect the polars (in which there is *no* disk to obscure the WD) to have similar colors. Perhaps the polars located at positions in the color-color diagram intermediate between the late main-sequence and the WD region *do* have substantial WD contributions diluting their IR luminosities. Cyclotron emission in the IR might also confuse the colors of polars.

Two IPs stand out because they are located in the polar-dominated region of the color-color diagram. The IP with $(H - K_s) \approx +0.15$ and $(J - H) \approx +0.55$ is the unusual magnetic propeller system AE Aqr (e.g., Wynn, King, & Horne 1995; Eracleous & Horne 1996), which may suffer from substantial intrinsic reddening due to ejected circumstellar material that affects its near-IR colors. The other outlying IP, with $(H - K_s) \approx +0.3$ and $(J - H) \approx +0.60$, is DO Dra, which is known to display considerable optical variability (e.g., Šimon 2000) and was in a faint state during its 2MASS observation (according to AAVSO and VSNET observations). During the faint state, the truncated disk of DO Dra may be substantially diminished or nonexistent, which allows the system to pass as a diskless polar. The single magnetic CV with $(H - K_s) < 0.0$ is the polar EU UMa. Its position in the color-color diagram is consistent

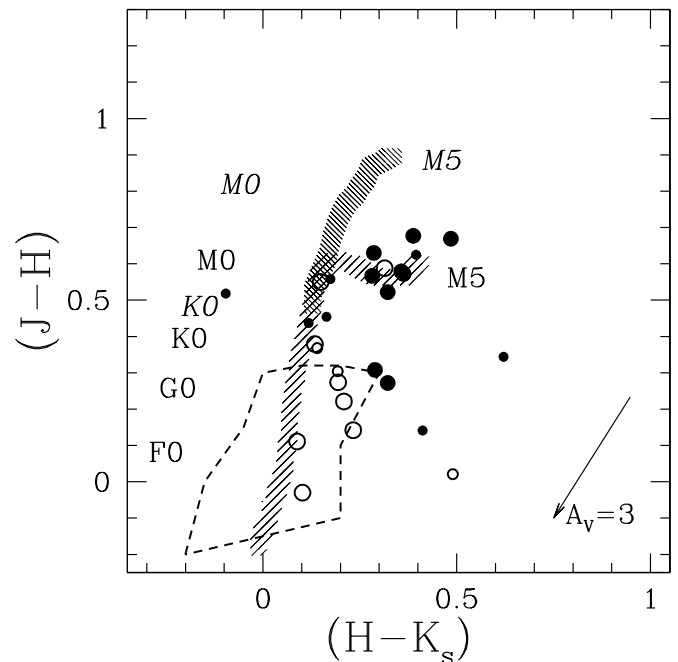


FIG. 6.—IR color-color diagram for magnetic CVs, as described in the caption to Fig. 4. Filled circles represent polars, open circles intermediate polars.

with that of the weak blue sequence noted for DNe in § 3.1.1. As with those systems, the reason for its anomalous near-IR colors is not entirely clear. EU UMa is a probable low-inclination ($i \leq 70^\circ$) polar discovered by *ROSAT* (Howell et al. 1995) and does not seem to have any (known) unusual characteristics that might account for its near-IR colors.

One polar and one IP are not shown in the figure because they lie outside the $(J-H)$ axis range. The polar is EF Eri, with $(H-K_s) = +0.30$ and $(J-H) = +1.54$, while the IP is XY Ari, with $(H-K_s) = +0.87$ and $(J-H) = +1.87$. EF Eri contains a degenerate, brown-dwarf-like secondary star and is probably a post-period-minimum CV (Howell & Ciardi 2001). (The similar system LL And, also studied by Howell & Ciardi 2001, was not detected by 2MASS.) EF Eri also has one of the coolest known WDs in a CV ($T_{\text{eff}} = 9500 \pm 500$ K; Beuermann et al. 2000). In addition, by comparison to contemporaneous AAVSO and VSNET observations, EF Eri may have been in a faint state during its 2MASS observation. All of these factors conspire to make EF Eri an extremely red CV, at least in the difference between the J and H bands. In the case of XY Ari, no optical brightness information is available at the time of its 2MASS observation. Allan, Hellier, & Ramseyer (1996) found brightness changes of up to $\Delta H \approx 0.6$ mag due to ellipsoidal variation of the secondary star, but this should presumably affect the J , H , and K bands similarly, so is not a likely explanation for the CV's extreme colors. However, XY Ari is somewhat unusual in being located behind the molecular cloud Lynds 1457 (Koyama et al. 1991; Boisson, Hameury, & Lasota 1992; Zuckerman et al. 1992, and others) and being the only known IP with a deep X-ray eclipse (Kamata, Tawara, & Koyama 1991; Hellier 1997). Both of these factors suggest that there is substantial reddening of the system (Zuckerman et al. 1992 estimate $A_V \sim 11.5$), which can explain its near-IR colors.

3.1.4. The Classical and Recurrent Novae

Figure 7 shows the data for novae. The shapes of the classical nova data points are coded according to their time since outburst (see figure caption for key). In general, the novae tend to follow the main sequence fairly closely in the color-color diagram. Most of the older novae ($\tau \gtrsim 75$ yr) have near-IR colors equivalent to F–K main-sequence stars. Novae are expected to resume DN outbursts some 50–200 yr after their nova outburst (e.g., Livio 1989; Warner 1995, chap. 4). The novae Q Cyg (1876; Bianchini 1990), and DI Lac (1910) and V841 Oph (1848; Hoard et al. 2000) have all displayed behavior that may be DN outbursts,⁸ and all three of these systems have near-IR colors from 2MASS that are consistent with mid-F to early-K main-sequence stars. We might expect some of the oldest novae in our sample to occupy the same region in the color-color diagram as DNe in outburst (if the former happened to be observed by 2MASS during a DN outburst), but this is not an adequate explanation for all of them. The potential influence of shells of circumstellar material ejected during the nova outbursts cannot be ignored here, although we would expect that, for example, IR emission from dust

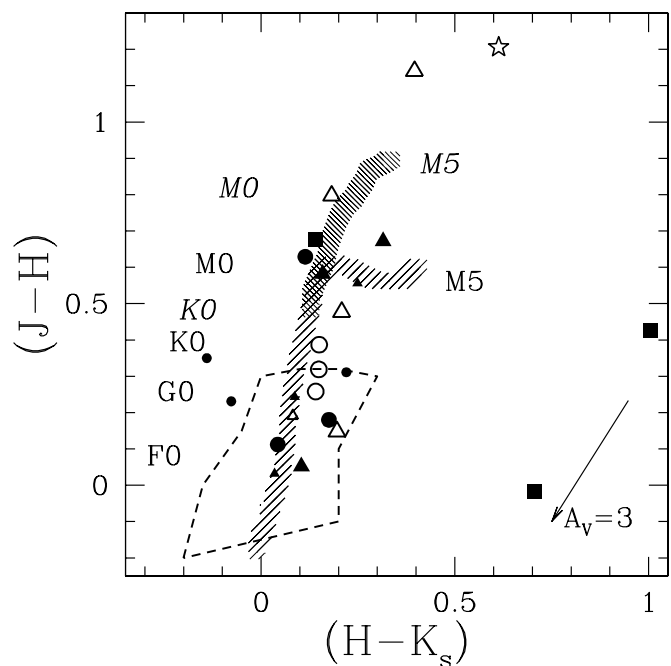


FIG. 7.—IR color-color diagram for classical novae, as described in the caption to Fig. 4. Points are coded according to the time since outburst of the nova, τ , as follows: filled squares: $\tau < 25$ yr; filled triangles: $\tau = 25$ –50 yr; open triangles: $\tau = 50$ –75 yr; filled circles: $\tau = 75$ –100 yr; open circles: $\tau > 100$ yr. The star-shaped point is the recurrent nova V745 Sco.

grains in the shells would enhance the red contribution to the nova luminosities rather than the blue. It is also possible that some of these systems may simply be misidentifications of normal F–K stars that are positionally coincident with old novae that have faded below the 2MASS detection limits.

The single star-shaped point in Figure 7 is the recurrent nova V745 Sco (recorded outbursts in 1937 and 1989). There are two types of recurrent novae: those with giant secondary stars and those with main-sequence (or only slightly evolved) secondary stars. V745 Sco is an example of the former, with a secondary star spectral type of M4–8 III (Anupama & Mikołajewska 1999). It is believed to have a distance of 4.6 kpc (Harrison, Johnson, & Spyromilio 1993), and its near-IR colors are consistent with an M5+ III star reddened by $A_V \approx 3$. However, it is not clear if this reddening is purely interstellar or intrinsic (or both), or if there is any contamination of the near-IR light by accretion processes. The classical nova located near V745 Sco in the diagram (with $J-H > +1.1$) is V1172 Sgr (1951). By comparison with V745 Sco, we expect that V1172 Sgr also contains a giant secondary star (and may even be an unrecognized recurrent nova). Weight et al. (1994) have also suggested this, although their discussion of the effect of the poorly known reddening of V1172 Sgr should be heeded. The other systems suggested to have giant secondary stars by Weight et al. (1994) are V3645 Sgr and EU Sct—the latter is not located in the 2IDR sky coverage, while we were unable to identify the near-IR counterpart of the former. V732 Sgr (1936; Gaposchkin 1955) has $H-K_s \approx +0.68$ and $J-H \approx +1.54$, and is not visible in the $(J-H)$ axis range displayed in Figure 7. It is another system located in this region of the color-color diagram. It may be a heavily reddened CV and/or have a giant secondary star.

⁸ Other novae that are believed to have resumed DN behavior are WY Sgr (not detected by 2MASS), V446 Her (we were unable to identify its 2MASS counterpart), and GK Per and V1017 Sgr (not in the 2IDR sky coverage).

Other well-known recurrent novae are RS Oph, T Pyx, and T CrB (see reviews in Webbink et al. 1987; Warner 1995, pp. 299–303); unfortunately, these systems are not included in the 2IDR sky coverage. Recurrent nova V394 CrA was not detected by 2MASS, while recurrent nova U Sco has only a 95% confidence upper limit of $K_s \gtrsim 15.3$ (and so is not included in our color-color diagram). Its J and H magnitudes differ by less than 0.05 mag from those reported by Hanes (1985), implying that his value of $K = 16.45$ is also accurate. This gives U Sco near-IR colors of $(H - K_s) \approx 0.0$ and $(J - H) \approx +0.4$. Harrison et al. (1993) have shown that JHK photometry can distinguish between the two types of recurrent novae. Systems with giant secondary stars have red near-IR colors (like V745 Sco), while systems with main-sequence or slightly evolved secondary stars are bluer (like U Sco). Two of the old novae, DN Gem (1912) and GR Sgr (1924), have $(H - K_s) < 0.0$, which places them near where U Sco (and T Pyx, another recurrent nova with a main-sequence secondary star) would be located in the color-color diagram (see also Harrison et al. 1993). Thus, it is possible that these two CVs are unrecognized U Sco-like recurrent novae. If so, then they either have very long recurrence times (> 80 – 90 yr), or subsequent outbursts have been missed.

Two of the three recent ($\tau < 25$ yr) novae, V4362 Sgr (1994) and V4633 Sgr (1998), have unusual near-IR colors that place them in the lower right corner of the color-color diagram (i.e., blue in $J - H$ but extremely red in $H - K_s$). V4362 Sgr is little studied, while V4633 Sgr is somewhat better observed (e.g., Liller & Jones 1999; Ashok & Chandrasekhar 2000; Venturini et al. 2000). The third young nova shown in the diagram is V977 Sco (1989), which appears to have “normal” near-IR colors. A fourth young nova detected by 2MASS, V838 Her (1991; e.g., Sugano et al. 1991; Chandrasekhar, Ashok, & Ragland 1992; Woodward et al. 1992), is not shown in the figure because it has only a 95% confidence upper limit magnitude in H . However, its corresponding near-IR colors are $(H - K_s) \gtrsim +0.7$ and $(J - H) \lesssim +0.5$, suggesting that it is also located in the lower right corner of the color-color diagram. We can suggest several possible explanations for the odd near-IR colors of these systems, although none of them is entirely satisfactory.

Photometric Uncertainty.—It is possible that the photometric uncertainties of these data are large enough to account for their odd position in the color-color diagram. However, inspection of the data in Table 1 shows that V4362 Sgr and V4633 Sgr actually have $\sigma < 0.1$ mag for their color indices. Thus, large photometric cannot be the sole cause of the extreme colors of these systems.

Reddening.—Because of the direction of the dereddening vector, even correcting for large interstellar reddening will not move these points close to the region of the color-color diagram occupied by the rest of the data.

Time Since Outburst.—V4633 Sgr was observed by 2MASS on 1998 July 19, approximately 4 months after its outburst on 1998 March 22 (Liller 1998). At this time, we should expect that the peak of the nova’s flux had moved well into the IR (~ 3 – $5 \mu\text{m}$; Gehrz 1988, e.g., see his Fig. 4), which could account for its extremely red near-IR colors. However, V4362 Sgr was observed by 2MASS ~ 4 yr after its outburst and V838 Her was observed ~ 7 yr after its

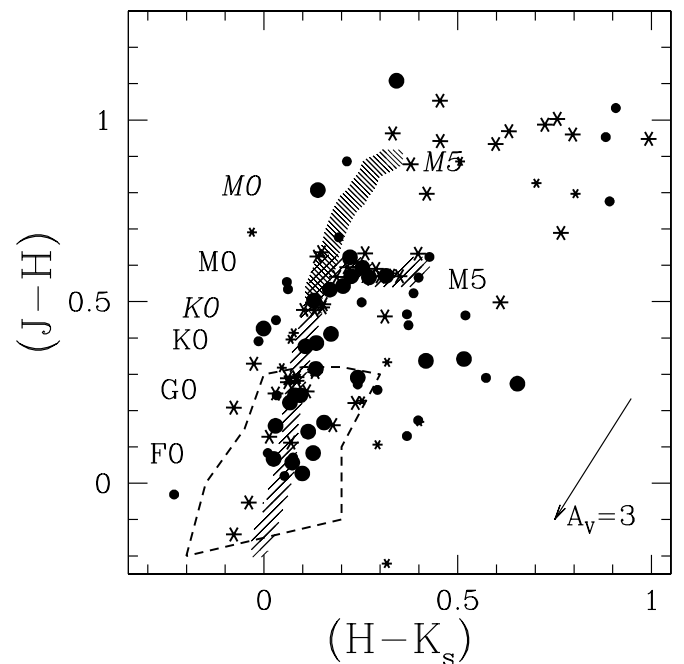


FIG. 8.—IR color-color diagram for uncertain/unclassified CVs, as described in the caption to Fig. 4. Filled circles show the CVs; asterisks show objects that have been reclassified as non-CV.

outburst, so it seems unlikely that the vestiges of the eruption were still affecting their near-IR colors to such a large extent.

Transient Behavior.—It is possible that the odd colors of these novae are the result of transient behavior, perhaps related to accretion disk instabilities and/or solar-type magnetic cycles on their secondary stars, and so on. Hoard et al. (2000) discuss a number of variability mechanisms that can affect old novae on different amplitude and time scales. Harrison (1992) shows four novae in the lower right corner of his near-IR color-color diagram:⁹ V1370 Aql, GW Lib, FH Ser, and CT Ser. The first three are not included in the 2IDR sky coverage; CT Ser has only a 95% confidence upper limit detection in K_s , corresponding to $(H - K_s) \lesssim +0.24$ and $(J - H) = +0.46$ (15). Even accounting for differences in photometric system, Harrison (1992) gives quite different color indices of $(H - K) = +0.91$ (27) and $(J - H) = -0.06$ (28) for CT Ser. Approximately 6 yr separate the observations made by Harrison (1992) in 1992 and the 2MASS observations in 1998. Since this is only an $\approx 10\%$ change in the age of the nova since its outburst in 1948, it does not seem likely that the large change in near-IR colors is due to an evolutionary change in CT Ser. Thus, it may be a temporary, transient phenomenon.

3.1.5. The Uncertain/Unclassified CVs

Figure 8 shows the data for uncertain/unclassified CVs. Many of these objects have near-IR colors consistent with main-sequence stars, and we expect that, in fact, at least some of them are misidentified normal stars. This figure also shows the data for targets from Downes et al. (2001) that were originally thought to be CVs, but have subsequently been reclassified as non-CV. By comparison with

⁹ Unfortunately, Harrison does not discuss these systems!

the colors of objects that are commonly mistaken for CVs, we can qualitatively assess the likelihood that the uncertain/unclassified systems are actually CVs. For example, objects located in the WD region coincident with the colors for main-sequence stars earlier than K-type might be NLs or DNe in outburst, but could also be misidentified normal main-sequence stars or WDs.

Many of the non-CV data points are found on the late main sequence; these are typically dMe flare stars whose H α emission and flaring activity, when little observational data is available, can be mistaken for the characteristic emission-line spectrum and variability of CVs. By comparison, we must suspect that at least some of the uncertain/unclassified CV data points that lie in this same region of the color-color diagram are actually dMe stars. If they *are* CVs, then these systems might be diskless polars that have near-IR colors indistinguishable from their underlying secondary stars (see § 3.1.3 and Fig. 6).

A similar case holds for Mira variables and symbiotic stars. These are located along the continuation of the giant branch at late spectral types (e.g., Whitelock & Munari 1992; Whitelock, Marang, & Feast 2000). There are a large number of non-CV objects in this region of the color-color diagram, which indicates that the weeding out of misidentified Mira variables and symbiotic stars from the ranks of the CVs has been very successful. Yet, a handful of nominal CVs also lie in this region ($J-H \gtrsim +0.75$), and at least some of these may actually be Mira variables or symbiotic stars. If they *are* CVs, then they could be reddened novae or recurrent novae (see § 3.1.4 and Fig. 7).

One object, V529 Ori, is not shown in Figure 8 because its near-IR colors ($H-K_s = +0.96$, $J-H = +1.33$) fall outside the displayed ($J-H$) axis range. V529 Ori is classified as a highly uncertain classical nova. Its year of outburst was originally thought to be 1667, but is more likely 1678 (Ashworth 1981). The optical counterpart of this nova was recently recovered (Robertson et al. 2000) after a number of other proposed counterparts were eliminated (e.g., Ringwald & Naylor 1997). The current optical and near-IR counterpart may truly be a heavily reddened nova, or it could be a misidentified symbiotic star (the known symbiotic star V2110 Oph, also not shown in the figure, has similar 2MASS colors, $H-K_s = +0.76$ and $J-H = +1.45$) or other type of emission-line object (as discussed in Robertson et al. 2000).

3.2. Color-Magnitude Diagram

The top panel of Figure 9 shows an IR color-magnitude diagram for CVs in our final data set. We used distances compiled from various literature sources (e.g., Berriman, Szkody, & Capps 1985; Warner 1987; Harrison & Gehrz 1988; Sproats et al. 1996; Shafter 1997) to convert K_s to M_{K_s} . We did not account for interstellar absorption, but expect this to be typically a small effect, generally resulting in an error in M_{K_s} of at most a few tenths of a magnitude (Cardelli, Clayton, & Mathis 1989). The thick line in the figure shows the main sequence, while the shaded region in the lower left of the top panel only is the approximate location of isolated WDs (which we derived using the data in Tables 1 and 3 of Leggett 1989). The fact that no CVs are located in the WD region of the color-magnitude diagram implies that the apparent agreement between many of the CVs and the WD region in the color-color diagrams is only due to a chance superposition of the CV colors with the

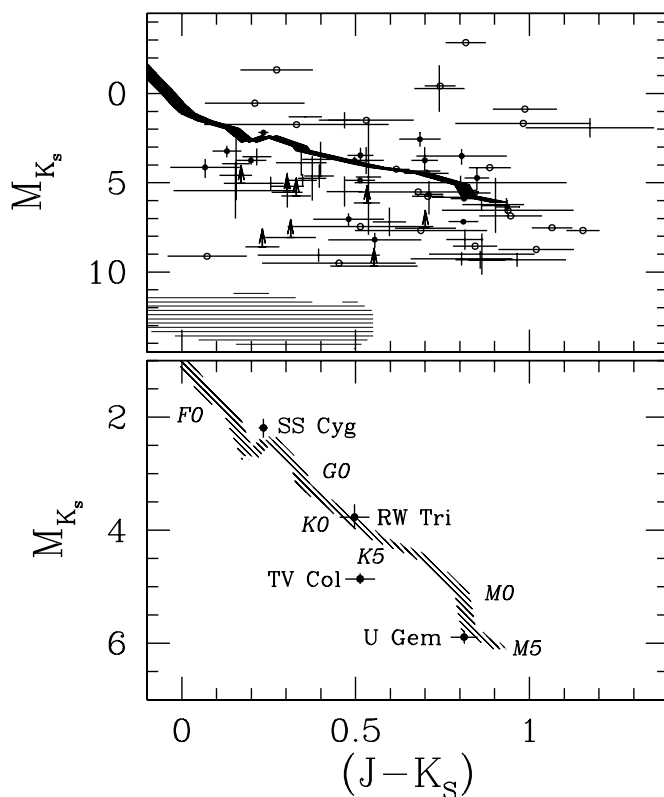


FIG. 9.—IR color-magnitude diagram for CVs. The thick line is the main sequence (Cox 2000, pp. 151–152) transformed to the 2MASS photometric system using the relations in Carpenter (2001), with positions of spectral types ranging from F0 to M5 labeled at the corresponding M_{K_s} value, but offset in $J-K_s$ (bottom panel only). The shaded region in the bottom left (top panel only) is the approximate location of isolated WDs (from data in Leggett 1989). In the top panel, filled symbols with error bars are from CVs with distances that have formal uncertainties; error bars only are from CVs with a distance range but no best value; open symbols with only horizontal error bars are from CVs with distance estimates only; and horizontal error bars with vertical arrows are from CVs with distance lower limits. Bottom panel shows four CVs with distances determined from their trigonometric parallaxes.

WD colors, rather than being caused by observing primarily the WD luminosity in the near-IR.

Unfortunately, if we assume that there should be some patterned distribution of CVs in the near-IR color-magnitude diagram, then the primary inference we can make from Figure 9 is that the distances to CVs are poorly known. The bottom panel of the figure, however, shows a close-up of the color-magnitude diagram, with spectral types labeled along the main sequence (at the correct M_{K_s} value but offset in $J-K_s$). Only four data points are included in this panel, for the CVs TV Col (IP), SS Cyg (DN), U Gem (DN), and RW Tri (NL). These systems have the distinction of having the most accurate and precisely known distances of all CVs. Their distances were determined from trigonometric parallaxes measured with the Fine Guidance Sensors on the *Hubble Space Telescope* (*HST*; see entry for each CV in the Appendix for distances and relevant literature references). It is very interesting (and somehow reassuring) that three of these four systems with the best known distances fall directly onto the main sequence in the color-magnitude diagram (and the fourth, TV Col, is not far off). At first inspection, this might lead one to believe that the near-IR observations did, in fact,

isolate the luminosity contribution of the CV secondary stars. It is immediately suspicious, however, that the implied secondary star spectral type for SS Cyg is approximately F5—quite early for a CV. In addition, SS Cyg was on the decline from outburst during its 2MASS observation (the other systems were at normal or quiescent brightness levels), so we should not a priori expect its secondary star to be a dominant contributor to the total system luminosity. Further analysis of this data in the next section demonstrates the importance of *not* utilizing color-magnitude diagrams as stand-alone diagnostic tools.

3.3. Orbital Period–Color Diagram

Figure 10 shows the $(J - K_s)$ data for CVs as a function of orbital period for all systems in our final data set with known P_{orb} . Smith & Dhillon (1998) compiled all known estimates of the secondary star spectral types in CVs with known orbital periods. They used 55 systems with “reliably determined” spectral types (defined as CVs in which features of the secondary star are visible in the optical spectrum and can be used to type the secondary star) to establish an empirical relationship between orbital period and expected secondary star spectral type. We have used the IR colors of main-sequence stars from Cox (2000) transformed to the 2MASS photometric system (Carpenter 2001) to plot the relationship between orbital period and the expected $(J - K_s)$ color of the secondary star as the thick curve in Figure 10. The horizontal bars in the figure are located at the $(J - K_s)$ value of the indicated spectral types, and show the range of orbital periods over which each secondary star spectral type is found (from Smith & Dhillon 1998).

If the near-IR data were truly isolating the secondary-star luminosity, then we would expect all of the data points to lie along the curve inside the range delimited by the bars. For

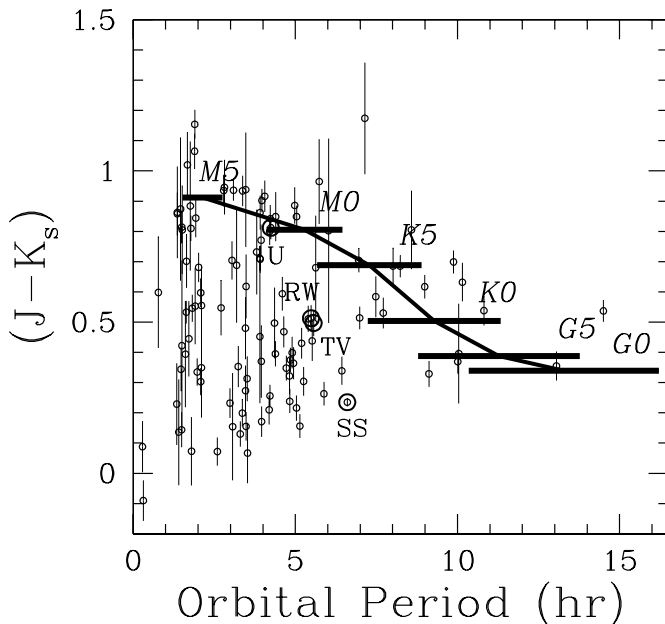


FIG. 10.—Orbital period-color diagram for CVs. The thick curve shows the expected $J - K_s$ color for CV secondary stars as a function of orbital period; the horizontal bars show the range of orbital period over which each CV secondary star spectral type is found. See § 3.3 for additional explanation.

long orbital period systems ($P_{\text{orb}} \gtrsim 7.5$ hr), this expectation is met fairly well. Admittedly, there are fewer CVs in this orbital period regime, but they are the systems with more massive, larger (and hence earlier spectral type) secondary stars. For short orbital period CVs, the majority of systems are significantly and systematically offset blueward of the expected $(J - K_s)$ color of their secondary stars. This blue contamination of their near-IR luminosities is almost certainly caused by the accretion process, through continuum and/or emission-line (e.g., Dhillon et al. 2000; Littlefair et al. 2000) contributions (see also Sproats et al. 1996).

We have highlighted the four CVs from Figure 9 (*bottom*) in Figure 10. The P_{orb} -color diagram shows that only U Gem has near-IR colors consistent with those of a secondary star with the spectral type expected for its orbital period (approximately M0). The true secondary star spectral type for U Gem, however, is M4 or later (Harrison et al. 2000), which indicates that U Gem is still bluer than the color of its secondary star. Despite the fact that it was located right on the main sequence in the color-magnitude diagram, SS Cyg would need $P_{\text{orb}} \gtrsim 15$ hr in order for its near-IR color to match the mid-F secondary star indicated by the color-magnitude diagram. Instead, we see that SS Cyg is substantially offset to the blue from the color of its predicted K5 secondary star. (SS Cyg is one of the systems used by Smith & Dhillon 1998 and actually does have a K5 secondary star.) With colors corresponding to a K0 star, RW Tri and TV Col are still somewhat offset, $\Delta(J - K_s) \approx 0.25$, from the near-IR color of their expected late-K to early-M secondary stars (K9.5 according to the relation in Smith & Dhillon 1998). This figure clearly reveals the curious fact that RW Tri and TV Col, an NL with a prominent disk and an IP with a truncated disk, have nearly identical $(J - K_s)$ colors to go along with their nearly identical orbital periods.

If we go further into the red by examining the $(H - K_s)$ color indices of these four CVs, we find that, while SS Cyg still has the color of an F star ($H - K_s \approx +0.05$), the colors of the other three systems have shifted to later spectral types. U Gem has $(H - K_s) \approx +0.24$, corresponding to a spectral type of approximately M2–3, and RW Tri and TV Col have $(H - K_s) \approx +0.13$, corresponding to a spectral type of approximately K3–4. These colors are still too blue to be truly representative of the secondary stars, but less so than for the $(J - K_s)$ index. The redder color indices appear to be converging toward the true spectral types of the secondary stars. This suggests that by observing CVs at even longer wavelengths (i.e., into the mid-IR), it might be possible to isolate the secondary-star luminosity.

Only a few points in Figure 10 are offset redward of the color expected for their secondary stars. It is possible, as suggested by Sproats et al. (1996), that these too-red CVs contain evolved secondary stars. They based this suggestion on only one system, DX And (which is not included in the 2IDR sky coverage). The secondary-star spectral type for DX And was determined to be K1 by Drew, Jones, & Woods (1993) via optical photometry and spectroscopy, and its $(J - K)$ color is consistent with a K1 giant. In our data set, AE Aqr and CH UMa are believed to have evolved secondary stars. The former shows a slight red IR color excess, while the latter does not (but the spectral types predicted by the relation of Smith & Dhillon 1998 for the orbital periods of both CVs are somewhat earlier than their observed secondary stars). On the other hand, there are

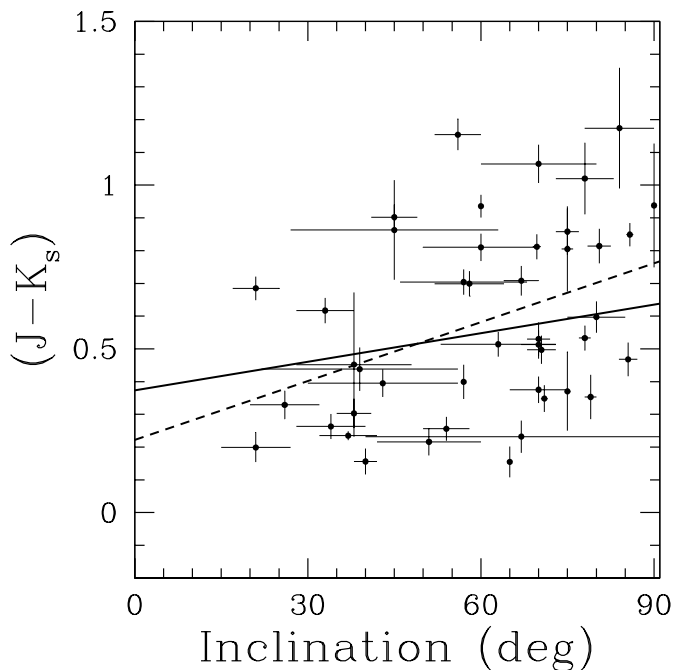


FIG. 11.—Inclination-color diagram for CVs. Inclinations are from Ritter & Kolb (1998) and references therein. The dashed line shows an unweighted linear fit to the data, while the solid line shows a linear fit to the data weighted by the inverse of the data uncertainties.

several CVs with red excesses in our data set that have been studied extensively and are not known or suspected of having evolved secondary stars (e.g., ST LMi, V838 Her, V841 Oph). Thus, there is a need for additional mechanisms to explain this effect.

We suggest that the cool outer regions of a prominent accretion disk are contributing to the near-IR luminosity in these systems. If this is the case, then we should expect that higher inclination systems (in which the cool disk edge is most visible and the hotter disk regions are most obscured) should be redder. For example, Knigge et al. (2000) have shown that the disk edge in CVs can have a substantial vertical extent and completely self-occult the inner disk and WD. In Figure 11, we have plotted the $(J - K_s)$ color (on the same scale as in Fig. 10) as a function of inclination for the CVs with inclination estimates compiled in Ritter & Kolb (1998). The dashed line is a linear fit to the data, while the solid line is a linear fit weighted by the inverses of the data uncertainties. There does appear to be at least a weak trend of redder systems at higher inclination.

4. SUMMARY

The observational data on CVs provided by 2MASS has proven to be a rich and deep reservoir of information. We anticipate the release of the final, full survey data in late 2002, and will revisit the analysis presented in this paper for the complete sample of CVs. In conclusion (for now), we summarize several of the important points revealed by this work:

1. Slightly less than half of all known CVs located in the 2IDR sky coverage were reliably detected by 2MASS with $S/N > 10$ in one or more of the near-IR bands at magnitude limits of $J \lesssim 15.8$, $H \lesssim 15.1$, and $K_s \lesssim 14.3$. About 10% of

these were detected with $S/N < 10$ as much as 1.0–1.5 mag fainter in one or more band(s).

2. Dwarf novae in outburst, nova-like CVs, and some old novae have near-IR colors similar to F–K main-sequence stars, although this does *not* imply that their secondary stars have spectral types of F–K.

3. Although some CVs have near-IR colors similar to isolated WDs, inspection of the colors of polars (which are dominated by their late main-sequence secondary stars and not by their bare WDs) and of the near-IR color-magnitude diagram (which shows all CVs with known distances to be brighter than the absolute K magnitudes of isolated WDs) demonstrates that this is purely coincidental. Not surprisingly, the exceptions to this are the interacting binary WDs.

4. In general, the expectation that observations in the near-IR will isolate the luminosity contribution of the secondary stars in CVs, and thereby allow the study of the mass donors in these interacting binaries, is *not* met. There is a significant and systematically blue contamination of the near-IR luminosities of most CVs by the accretion process. The exceptions to this are the polars, which have near-IR colors completely consistent with late (M0+) main-sequence stars. This has important implications for past treatments of near-IR observations of CVs. For example, the assumption that the K magnitude is that of the secondary star and can be used to estimate the distance (e.g., Bailey's method; Bailey 1981) must now be considered highly suspect for the vast majority of CVs. Although still too blue to be the pure secondary star, the $(H - K_s)$ color indices correspond to later spectral types than the $(J - K_s)$ indices, indicating a decrease in the contamination by the accretion process. Thus, it is possible that observations at longer (mid-IR) wavelengths could succeed in isolating the secondary stars.

5. Modeling of the disk contribution in the near-IR, which could then be subtracted from the observed data to isolate the secondary star contribution, offers a means of untangling the luminosities of the CV components. Ciardi et al. (1998) have made some promising first steps in this area. Robust CV modeling techniques and software routines now exist that are, in principle, applicable to the near-IR regime (e.g., TLUSTY + BINSYN; Linnell & Hubeny 1996). However, they are currently hampered by the relative simplicity of model atmospheres/synthetic spectra appropriate for cool ($T \lesssim$ a few thousand K) environments (A. P. Linnell 2001, private communication). Additional work incorporating a realistic and comprehensive treatment of molecular transitions (such as TiO), as well as the influence of dust grains, is required before successful modeling of CVs in the near-IR can be accomplished (e.g., Allard et al. 1997 and references therein).

6. A few CVs are redder than the color of the secondary-star spectral type expected at their orbital period. The presence of an evolved secondary star or the luminosity contribution of the cool outer regions of a prominent accretion disk might produce this effect. In the latter case, the red excess should be more pronounced in CVs viewed close to edge-on. There is at least a weak trend of redder color at higher inclination that supports this.

7. In all the near-IR color-color diagrams of CV subclasses, there are loci of data with unusual, unexplained colors. Clearly, additional IR observations of CVs (especially time-resolved over orbital and longer timescales) are needed.

This publication makes use of data products from the 2 Micron All Sky Survey, which is a joint project of the University of Massachusetts and the Infrared Processing and Analysis Center/California Institute of Technology, funded by the National Aeronautics and Space Administration and the National Science Foundation. It also utilized NASA's Astrophysics Data System Abstract Service and the SIMBAD database operated by CDS, Strasbourg, France, as well as images from the Digitized Sky Survey, which was produced at the Space Telescope Science Institute under US Government grant NAG W-2166. (The images of these surveys are based on photographic data obtained using the Oschin Schmidt Telescope on Palomar Mountain and the UK Schmidt Telescope. The plates were processed into the

present compressed digital form with the permission of these institutions.) Data compiled on the Web sites of the American Association of Variable Star Observers and the Variable Star Network were used to qualitatively estimate the optical brightness states of the CVs at the times of observation by 2MASS. The conceptualization and completion of this project was greatly aided by the Catalog and Atlas of CVs, 1st ed. (Downes & Shara 1993), 2d ed. (Downes et al. 1997), and, especially, the Living Edition¹⁰ (Downes et al. 2001). We thank the anonymous referee, whose comments were helpful in improving the presentation of this work.

¹⁰ See <http://icarus.stsci.edu/~downes/cvcat/>.

APPENDIX A

COMMENTS ON SELECTED TARGETS

This appendix contains comments primarily pertaining to the near-IR finding charts shown in Figure 1 and the CVs not detected by 2MASS. Some of these comments correspond to entries in the CV catalog of Downes et al. (2001). We caution that since the latter is a “living” Web-based document, our comments here may become outdated as the Downes et al. (2001) catalog is updated in the future. (During the revision of this manuscript prior to publication, we performed a final check of the targets listed below. Comments given in *italic* reflect updates to the Downes et al. [2001] catalog as of 2001 August 22.) We also list “reliable” (i.e., spectroscopically determined) secondary-star spectral types (as in Beuermann et al. 1998 and Smith & Dhillon 1998) where available. Additional discussion of some individual objects is included in § 3.

RX And.—Secondary star is K5V or earlier (Dhillon & Marsh 1995).

LS And.—Not detected by 2MASS; Szkody (1994) reports $J > 18$.

OS And.—Not detected by 2MASS; Szkody (1994) reports $J = 17.8$ (1) and $K > 15$.

PQ And.—Not detected by 2MASS; Sproats et al. (1996) report $J = 18.51$ (25) and $K = 17.66$ (24).

AE Aqr.—Secondary star is K4–5V, evolved (Welsh, Horne, & Gomer 1993; Casares et al. 1996).

EG Aqr.—Not detected by 2MASS; Sproats et al. (1996) report $J = 17.10$ (20) and $K = 16.26$ (19).

HU Aqr.—Secondary star is M4 V (Glenn et al. 1994).

UU Aql.—Secondary star is M2–4 V (Connon Smith et al. 1997).

XY Ari.—No optical chart or chart reference in Downes et al. (2001). Secondary star is spectral type K8 (Allan et al. 1996).

SS Aur.—Distance from astrometric parallax measured with *HST* Fine Guidance Sensors, $d = 200.0$ (25.7) pc (Harrison et al. 1999). Secondary star is M1 V (Harrison et al. 2000, and references therein).

V363 Aur.—Secondary star is late-G V to early-K V (Schlegel, Honeycutt, & Kaitchuck 1986).

Cam (05^h57^m24^s, +72°41'52").—No optical chart or chart reference in Downes et al. (2001). *Downes et al. (2001) now contains an optical chart matching our IR chart.*

Cam (05^h58^m18^s, +67°53'46").—Close visual companion to the northeast in the optical is not detected in the 2MASS images.

Z Cam.—Secondary star is K7 V (Szkody & Wade 1981).

HS Cam.—Secondary star is M4–6 V (Tovmassian et al. 1997).

Cnc (08^h06^m22^s, +15°27'15").—The coordinates given for this CV correspond to the bright star southwest of the position indicated in the optical chart in Downes et al. (2001) and the original chart in Israel et al. (1999b). The CV is not detected by 2MASS. *Correct coordinates (08^h06^m23^s, +15°27'31") are now listed in Downes et al. (2001).*

AR Cnc.—Secondary star is M4–5.5 V (Mukai et al. 1990).

AT Cnc.—Secondary star is K7–M0 V (Connon Smith et al. 1997).

WW Cet.—Secondary star is M2–3 V (Hawkins, Smith, & Jones 1990).

WX Cet.—Not detected by 2MASS; Szkody & Feinswog (1988) report $J = 17.09$ (5) and $H = 17.14$ (15).

TV Col.—Distance from astrometric parallax measured with *HST* Fine Guidance Sensors, $d = 368_{-15}^{+17}$ pc (McArthur et al. 2001).

AL Com.—Based on the optical chart and position in Howell et al. (1996), the near-IR source close to the position of AL Com in the 2MASS images is the close visual companion to the southeast in the Howell et al. chart. AL Com itself was not detected by 2MASS. Near-IR magnitudes range from $J = 13.23$ (2) and $K = 13.12$ (2) in superoutburst (Howell et al. 1996) to $J = 16.79$ (20) and $K = 15.96$ (18) in quiescence (Sproats et al. 1996).

V394 CrA.—Not detected by 2MASS; Harrison et al. (1993) report $K > 14.0$.

Cyg (19^h58^m14^s, +32°32'41").—Optical chart in Downes et al. (2001) indicates west component of close visual pair; however, original chart and coordinates in Israel et al. (1999a) indicate east component, as shown in our near-IR chart. *Optical chart in Downes et al. (2001) now agrees with Israel et al. (1999a).*

Cyg (20^h15^m15^s, +36°59'24").—Orientation of optical finding chart in Halpern et al. (2001) is given incorrectly in the caption to their Figure 4; actual orientation is east at the top and north to the right.

- Cyg* ($20^{\text{h}}15^{\text{m}}36^{\text{s}}$, $+37^{\circ}04'57''$).—Same comment as for *Cyg* ($20^{\text{h}}15^{\text{m}}15^{\text{s}}$, $+36^{\circ}59'24''$).
- Cyg* ($20^{\text{h}}15^{\text{m}}37^{\text{s}}$, $+37^{\circ}11'23''$).—Same comment as for *Cyg* ($20^{\text{h}}15^{\text{m}}15^{\text{s}}$, $+36^{\circ}59'24''$).
- Cyg* ($21^{\text{h}}30^{\text{m}}18^{\text{s}}$, $+47^{\circ}10'07''$).—Coordinates of X-ray counterpart proposed in Motch et al. (1997) are $21^{\text{h}}30^{\text{m}}18^{\text{s}}.5$, $+47^{\circ}10'07''.3$ (J2000); this star is indicated in our near-IR chart. The coordinates given in Downes et al. (2001) ($21^{\text{h}}30^{\text{m}}21^{\text{s}}$, $+47^{\circ}09'53''$, J2000) correspond to the faint star to the southeast of the CV. *Correct coordinates are now given in Downes et al. (2001).*
- SS Cyg*.—Distance from astrometric parallax measured with *HST* Fine Guidance Sensors, $d = 166.2$ (12.7) pc (Harrison et al. 1999). 2MASS data obtained during decline from outburst; near-IR magnitudes in quiescence reported as $J = 10.10$ (4), $H = 9.78$ (4), and $K = 9.35$ (4) (Berriman et al. 1985). Secondary star is K5 V (Hessman et al. 1984).
- EM Cyg*.—Secondary star is K5 V (Stover, Robinson, & Nather 1981).
- EY Cyg*.—Secondary star is K5–M0 V (Connon Smith et al. 1997).
- V450 Cyg*.—Close visual companion $\approx 3''$ to the northeast in optical is detected in near-IR by 2MASS, but the CV is not.
- V465 Cyg*.—Not detected by 2MASS; Szkody (1994) reports $J > 18$.
- V503 Cyg*.—Close visual companion to the southwest is brighter than the CV in near-IR (opposite compared to the optical). CV is very faint in J ; 95% confidence upper limits in H and K_s .
- V823 Cyg*.—Very faint; 95% confidence upper limit in K_s .
- V1114 Cyg*.—Apparently unrelated IR source detected in JHK_s at $\approx 2''.5$ north of optical position. This star is not detected in the optical DSS first and second generation images, whereas the CV is clearly seen in the optical at the correct position. Possible faint (blended) detection of the CV in K_s only at the optical position.
- V1668 Cyg*.—Not detected by 2MASS; Szkody (1994) reports $J > 18$.
- V1819 Cyg*.—Very faint (undetected) IR source near optical position; however, it is unclear whether this is the CV or its close companion to the northwest that is visible in optical finding charts (and which would be blended in the 2MASS images).
- DM Dra*.—Not detected by 2MASS; Sproats et al. (1996) report $J = 18.60$ (19).
- DO Dra*.—Secondary star is M4V (Haswell et al. 1997; Mukai et al. 1990).
- DV Dra*.—Not detected by 2MASS; Sproats et al. (1996) report $J = 16.98$ (21) and $K = 16.23$ (19).
- EX Dra*.—Secondary star is M1–2 V (Billington, Marsh, & Dhillon 1996).
- Eri* ($03^{\text{h}}54^{\text{m}}10^{\text{s}}$, $-16^{\circ}52'50''$).—No optical chart or chart reference in Downes et al. (2001). Faint; 95% confidence upper limit in K_s . *Downes et al. (2001) now contains an optical chart matching our IR chart.*
- XZ Eri*.—Not detected by 2MASS; Sproats et al. (1996) report $J = 15.00$ (14) and $K = 14.04$ (11).
- AH Eri*.—Considerable variability in near-IR magnitudes reported in the literature; e.g., $J = 14.8$ (2)–16.44 (6) (Szkody 1987; Szkody & Mateo 1986, respectively). Secondary star is M3–5 V (Howell, Liebert, & Mason 1994; Thorstensen 1997).
- UZ For*.—Secondary star is M4.5 V (Beuermann, Thomas, & Schwöpe 1988).
- VY For*.—Secondary star is M4.5 V (Beuermann et al. 1989).
- U Gem*.—Distance from astrometric parallax measured with *HST* Fine Guidance Sensors, $d = 96.4$ (4.6) pc (Harrison et al. 1999). Secondary star is M4 V or later (Harrison et al. 2000, and references therein).
- DM Gem*.—Not detected by 2MASS; Szkody (1994) reports $J = 16.9$ (1).
- PQ Gem*.—Faint close visual companion $\approx 3''$ west also detected by 2MASS.
- AM Her*.—Secondary star is M4 or later (Young, Schneider, & Schectman 1981).
- DQ Her*.—Secondary star is M3 or later (Young & Schneider 1981).
- V446 Her*.—A known close visual triple (Honeycutt et al. 1998) that is blended in the 2MASS images.
- EX Hya*.—Secondary star is M3 V (Dhillon et al. 1997).
- BL Hyi*.—Secondary star is M3–4 V (Visvanathan, Bessell, & Wickramasinghe 1984).
- Leo* ($09^{\text{h}}24^{\text{m}}56^{\text{s}}$, $+13^{\circ}20'52''$).—No optical chart or chart reference in Downes et al. (2001). *Downes et al. (2001) now contains an optical chart matching our IR chart; however, those authors suspect that the indicated star is too bright to be the CV. On the other hand, this system is classified as a polar, and we note that its near-IR colors are completely consistent with those of other polars.*
- U Leo*.—Not detected by 2MASS; Szkody (1994) reports $J = 16.4$ (1) and $K = 15.9$ (0.1).
- X Leo*.—Considerable variability in near-IR magnitudes reported in the literature; e.g., $J = 12.63$ (2)–14.16 (2) (Szkody 1987; Szkody & Mateo 1986, respectively).
- LMi* ($10^{\text{h}}26^{\text{m}}27^{\text{s}}$, $+38^{\circ}45'01''$).—No optical chart or chart reference in Downes et al. (2001). *Downes et al. (2001) now contains an optical chart matching our IR chart.*
- ST LMi*.—Secondary star is M3–6 V (Howell et al. 2000).
- MV Lyr*.—Secondary star is M5 V (Skillman, Patterson, & Thorstensen 1995).
- V369 Lyr*.—Coordinates ($19^{\text{h}}11^{\text{m}}55^{\text{s}}$, $+32^{\circ}12'07''$, J2000) and star indicated in finding chart in Downes et al. (2001) do not match (no star in optical chart at these coordinates). The star indicated in both the Downes et al. (2001) optical finding chart and our near-IR chart has coordinates $19^{\text{h}}11^{\text{m}}56^{\text{s}}.3$, $+32^{\circ}12'00''.4$ (J2000). *Status in Downes et al. (2001) has now been revised to “no candidate.”*
- BT Mon*.—Secondary star is G8 V (Smith, Dhillon, & Marsh 1998).
- KQ Mon*.—Close visual triple (resolved in 2MASS images).
- V2110 Oph*.—Confirmed as symbiotic star (e.g., Ringwald, Naylor, & Mukai 1996, and others).
- CN Ori*.—Secondary star is M4 V (Friend et al. 1990a).
- CZ Ori*.—Secondary star is $M2.5 \pm 1.0$ V (Ringwald, Thorstensen, & Hamwey 1994).
- V529 Ori*.—Coordinates in Downes et al. (2001) ($05^{\text{h}}58^{\text{m}}22^{\text{s}}.3$, $+20^{\circ}15'26''$, J2000) are incorrect. Robertson et al. (2000) identify CV at correct position as indicated in our near-IR chart at $05^{\text{h}}58^{\text{m}}20^{\text{s}}.1$, $+20^{\circ}15'45''.2$ (J2000). *Coordinates and optical chart in Downes et al. (2001) now match Robertson et al. (2000).*

- RU Peg.*—Secondary star is K3 V (Wade 1982; Friend et al. 1990b).
KT Per.—Secondary star is M3.3 V (Thorstensen & Ringwald 1997).
V400 Per.—Not detected by 2MASS; Szkody (1994) reports $J > 18.4$.
DY Pup.—Not detected by 2MASS; Szkody (1994) reports $J > 18.4$.
WY Sge.—Not detected by 2MASS; Somers, Mukai, & Naylor (1996) report $J = 16.120$ (7), $H = 15.735$ (9), and $K = 15.486$ (7).
GR Sgr.—Close visual companion $\approx 3''5$ to the southeast.
V759 Sgr.—Near-IR counterpart not identified because of crowding; at least two blended 2MASS sources coincident with optical coordinates.
V990 Sgr.—CV could be any (or none) of the near-IR sources circled in our chart.
V2468 Sgr.—Bright *JHK* magnitudes may indicate that this star is a long-period variable (Downes et al. 2001).
V3889 Sgr.—CV is undetected on both the optical chart in Downes et al. (2001) and our near-IR chart.
V4074 Sgr.—Part of a visual triple system that is blended in 2MASS. Many literature sources classify V4074 Sgr as a symbiotic star (e.g., Belczyński et al. 2000 and references therein).
V4362 Sgr.—No optical chart or chart reference in Downes et al. (2001). Downes et al. (2001) now contains an optical chart, but they find “no candidate.” The 2MASS image shows a brighter object at the correct coordinates.
U Sco.—Secondary star is late-F V to early-G V, slightly evolved (Hanes 1985; Schaefer 1990; Johnston & Kulkarni 1992).
V734 Sco.—Classified as a nova or possible Mira variable (Downes et al. 2001); bright near-IR counterpart suggests the latter may be correct.
V745 Sco.—Optical finding chart in Downes et al. (2001) shows incorrect position; correct object is indicated in our near-IR chart from the optical identification in Sekiguchi et al. (1990). Downes et al. (2001) chart now matches Sekiguchi et al. (1990).
FV Sct.—Not detected by 2MASS; Szkody (1994) reports $J = 17.3$ (1).
QZ Ser.—No optical chart or chart reference in Downes et al. (2001); however, those authors note that the spectrum of the object at the given coordinates is a G star. Downes et al. (2001) now contains an optical chart matching our IR chart; however, identification is still in doubt.
Sex ($10^h 39^m 47^s$, $-05^{\circ} 06' 58''$).—No optical chart or chart reference in Downes et al. (2001). Downes et al. (2001) now contains an optical chart matching our IR chart.
XX Tau.—Not detected by 2MASS; Szkody (1994) reports $J = 17.3$ (1).
RW Tri.—Distance from astrometric parallax measured with *HST* Fine Guidance Sensors, $d = 341^{+38}_{-31}$ pc (McArthur et al. 1999).
AI Tri.—Secondary star is M2.5 V (Schwarz et al. 1998).
UX UMa.—Secondary star is M0 V (Rutten et al. 1994).
AR UMa.—Secondary star is M6 V (Remillard, Schacter, & Silber 1994).
CH UMa.—Secondary star is M0 V, evolved (Friend et al. 1990b).
DV UMa.—Not detected by 2MASS; Sproats et al. (1996) report $K = 16.10$ (18). Secondary star is $\sim M4.5$ V (Mukai et al. 1990).
FY Vul.—Note that the apparent faint, close visual companion to the south in our near-IR chart is not detected in optical.
PW Vul.—Part of visual triple (e.g., Ringwald & Naylor 1996) that is blended in 2MASS.

REFERENCES

- Abbott, T. M. C., Shafter, A. W., Wood, J. H., Tomaney, A. B., & Haswell, C. A. 1990, *PASP*, 102, 558
Allan, A., Hellier, C., & Ramseyer, T. F. 1996, *MNRAS*, 282, 699
Allard, F., Hauschildt, P. H., Alexander, D. R., & Starrfield, S. 1997, *ARA&A*, 35, 137
Ashok, N. M., & Chandrasekhar, T. 2000, *Bull. Astron. Soc. India*, 28, 265
Ashworth, W. B., Jr. 1981, *QJRAS*, 22, 22
Anupama, G. C., & Mikołajewska, J. 1999, *A&A*, 344, 177
Bailey, J. 1981, *MNRAS*, 197, 31
Belczyński, K., Mikołajewska, J., Munari, U., Ivison, R. J., & Friedjung, M. 2000, *A&AS*, 146, 407
Bergeron, P., Leggett, S. K., & Ruiz, M. 2001, *ApJS*, 133, 413
Berriman, G., Szkody, P., & Capps, R. W. 1985, *MNRAS*, 217, 327
Beuermann, K., Baraffe, I., Kolb, U., & Weichold, M. 1998, *A&A*, 339, 518
Beuermann, K., Thomas, H.-C., Giommi, P., Tagliaferri, G., & Schwöpe, A. D. 1989, *A&A*, 219, L7
Beuermann, K., Thomas, H.-C., & Schwöpe, A. 1988, *A&A*, 195, L15
Beuermann, K., Wheatley, P., Ramsay, G., Euchner, F., & Gänsicke, B. T. 2000, *A&A*, 354, L49
Bianchini, A. 1990, *AJ*, 99, 1941
Billington, I., Marsh, T. R., & Dhillon, V. S. 1996, *MNRAS*, 278, 673
Boisson, C., Hameury, J. M., & Lasota, J. P. 1992, *Acta Astron.*, 42, 377
Cardelli, J. A., Clayton, G. C., & Mathis, J. S. 1989, *ApJ*, 345, 245
Carpenter, J. M. 2001, *AJ*, 121, 2851
Casares, J., Mouchet, M., Martínez-Pais, I. G., & Harlaftis, E. T. 1996, *MNRAS*, 282, 182
Chandrasekhar, T., Ashok, N. M., & Ragland, S. 1992, *MNRAS*, 255, 412
Ciardi, D. R., Howell, S. B., Hauschildt, P. H., & Allard, F. 1998, *ApJ*, 504, 450
Cannon Smith, R., Sarna, M. J., Catalán, M. S., & Jones, D. H. P. 1997, *MNRAS*, 287, 271
Cox, A. N. 2000, *Allen's Astrophysical Quantities* (4th Ed.; New York: Springer)
Dahlmark, L. 1996, *Inf. Bull. Variable Stars*, 4329, 1
Dhillon, V. S., Littlefair, S. P., Howell, S. B., Ciardi, D. R., Harrop-Allin, M. K., & Marsh, T. R. 2000, *MNRAS*, 314, 826
Dhillon, V. S., & Marsh, T. R. 1995, *MNRAS*, 275, 89
Dhillon, V. S., Marsh, T. R., Duck, S. R., & Rosen, S. R. 1997, *MNRAS*, 285, 95
Downes, R. A., & Shara, M. M. 1993, *PASP*, 105, 127
Downes, R. A., Webbink, R. F., & Shara, M. M. 1997, *PASP*, 109, 345
Downes, R. A., Webbink, R. F., Shara, M. M., Ritter, H., Kolb, U., & Duerbeck, H. W. 2001, *PASP*, 113, 764
Drew, J. E., Jones, D. H. P., & Woods, J. A. 1993, *MNRAS*, 260, 803
Eracleous, M., & Horne, K. 1996, *ApJ*, 471, 427
Friend, M. T., Martin, J. S., Smith, R. C., & Jones, D. H. P. 1990a, *MNRAS*, 246, 637
—, 1990b, *MNRAS*, 246, 654
Gaposchkin, S. 1955, *AJ*, 60, 454
Gehrz, R. D. 1988, *ARA&A*, 26, 377
Glenn, J., Howell, S. B., Schmidt, G. D., Liebert, J., Grauer, A. D., & Wagner, R. M. 1994, *ApJ*, 424, 967
Green, P. J., Ali, B., & Napiwotzki, R. 2000, *ApJ*, 540, 992
Halpern, J. P., Eracleous, M., Mukherjee, R., & Gotthelf, E. V. 2001, *ApJ*, 551, 1016
Handler, G., et al. 1997, *A&A*, 320, 125
Hanes, D. A. 1985, *MNRAS*, 213, 443
Harrison, T. E. 1992, *MNRAS*, 259, 17P
Harrison, T. E., & Gehrz, R. D. 1988, *AJ*, 96, 1001
Harrison, T. E., Johnson, J. J., & Spyromilio, J. 1993, *AJ*, 105, 320
Harrison, T. E., McNamara, B. J., Szkody, P., & Gilliland, R. L. 2000, *AJ*, 120, 2649

- Harrison, T. E., McNamara, B. J., Szkody, P., McArthur, B. E., Benedict, G. F., Klemola, A. R., & Gilliland, R. L. 1999, *ApJ*, 515, L93
- Haswell, C. A., Patterson, J., Thorstensen, J. R., Hellier, C., & Skillman, D. R. 1997, *ApJ*, 476, 847
- Hawkins, N. A., Smith, R. C., & Jones, D. H. P. 1990, in *Accretion Powered Compact Binaries*, ed. C. Mauche (Cambridge: Cambridge Univ. Press), 113
- Hellier, C. 1997, *MNRAS*, 291, 71
- Hessman, F. V., Robinson, E. L., Nather, R. E., & Zhang, E.-H. 1984, *ApJ*, 286, 747
- Hoard, D. W., Szkody, P., Honeycutt, R. K., Robertson, J., Desai, V., & Hillwig, T. 2000, *PASP*, 112, 1595
- Honeycutt, R. K., Robertson, J. W., Turner, G. W., & Henden, A. A. 1998, *ApJ*, 495, 933
- Howell, S. B., & Ciardi, D. R. 2001, *ApJ*, 550, L57
- Howell, S. B., Ciardi, D. R., Dhillon, V. S., & Skidmore, W. 2000, *ApJ*, 530, 904
- Howell, S. B., Deyoung, J., Mattei, J. A., Foster, G., Szkody, P., Cannizzo, J. K., Walker, G., & Fierce, E. 1996, *AJ*, 111, 2367
- Howell, S. B., Liebert, J., & Mason, K. O. 1994, *Inf. Bull. Variable Stars*, 4072, 1
- Howell, S. B., Sirk, M. M., Malina, R. F., Mittaz, J. P. D., & Mason, K. O. 1995, *ApJ*, 439, 991
- Israel, G. L., Covino, S., Polcaro, V. F., & Stella, L. 1999a, *A&A*, 345, L1
- Israel, G. L., Panzera, M. R., Campana, S., Lazzati, D., Covino, S., Tagliaferrri, G., & Stella, L. 1999b, *A&A*, 349, L1
- Johnston, H. M., & Kulkarni, S. R. 1992, *ApJ*, 396, 267
- Kamata, Y., Tawara, Y., & Koyama, K. 1991, *ApJ*, 379, L65
- Knigge, C., Long, K. S., Hoard, D. W., Szkody, P., & Dhillon, V. S. 2000, *ApJ*, 539, L49
- Koyama, K., et al. 1991, *ApJ*, 377, 240
- Leggett, S. K. 1989, *A&A*, 208, 141
- Liller, W. 1998, *IAU Circ.*, 6846, 1
- Liller, W., & Jones, A. F. 1999, *Inf. Bull. Variable Stars*, 4664, 1
- Linnell, A. P., & Hubeny, I. 1996, *ApJ*, 471, 958
- Littlefair, S. P., Dhillon, V. S., Howell, S. B., & Ciardi, D. R. 2000, *MNRAS*, 313, 117
- Livio, M. 1989, in *Proc. IAU Colloq. 122, Physics of Classical Novae*, ed. A. Cassatella & R. Viotti (Berlin: Springer), 342
- Marsh, T. R. 1999, *MNRAS*, 304, 443
- McArthur, B. E., et al. 1999, *ApJ*, 520, L59
- . 2001, *ApJ*, 560, 907
- Motch, C., Guillout, P., Haberl, F., Pakull, M. W., Peitsch, W., & Reinsch, K. 1997, *A&AS*, 122, 201
- Mukai, K., et al. 1990, *MNRAS*, 245, 385
- O'Donoghue, D., Fairall, A. P., & Warner, B. 1987, *MNRAS*, 225, 43
- Ramseyer, T. F., Dinerstein, H. L., Lester, D. F., & Provencal, J. 1993, *AJ*, 106, 1191
- Reimers, D. 1985, *A&A*, 142, L16
- Remillard, R. A., Schacter, J. F., & Silber, A. D. 1994, *ApJ*, 426, 288
- Ringwald, F. A., & Naylor, T. 1996, *MNRAS*, 278, 808
- . 1997, *A&A*, 326, 629
- Ringwald, F. A., Naylor, T., & Mukai, K. 1996, *MNRAS*, 281, 192
- Ringwald, F. A., Thorstensen, J. R., & Hamwey, R. M. 1994, *MNRAS*, 271, 323
- Ritter, H., & Kolb, U. 1998, *A&AS*, 129, 83
- Robertson, J. W., Honeycutt, R. K., Hillwig, T., Jurcevic, J. S., & Henden, A. A. 2000, *AJ*, 119, 1365
- Rutten, R. G. M., Dhillon, V. S., Horne, K., & Kuulkers, E. 1994, *A&A*, 283, 441
- Schaefer, B. E. 1990, *ApJ*, 355, L39
- Schlegel, E. M., Honeycutt, R. K., & Kaitchuck, R. H. 1986, *ApJ*, 307, 760
- Schwarz, R., et al. 1998, *A&A*, 338, 465
- Sekiguchi, K., et al. 1990, *MNRAS*, 246, 78
- Shafter, A. W. 1983, *ApJ*, 267, 222
- . 1992, *ApJ*, 394, 268
- . 1997, *ApJ*, 487, 226
- Sherrington, M. R., & Jameson, R. F. 1983, *MNRAS*, 205, 265
- Sherrington, M. R., Jameson, R. F., & Bailey, J. 1984, *MNRAS*, 206, 859
- Simon, V. 2000, *A&A*, 360, 627
- Skillman, D. R., Patterson, J., & Thorstensen, J. R. 1995, *PASP*, 107, 545
- Skrutskie, M. F., et al. 1995, *BAAS*, 187, 75.07
- . 1997, in *The Impact of Large Scale Near-IR Sky Surveys*, ed. F. Garzon et al. (Dordrecht: Kluwer), 25
- Smith, D. A., & Dhillon, V. S. 1998, *MNRAS*, 301, 767
- Smith, D. A., Dhillon, V. S., & Marsh, T. R. 1998, *MNRAS*, 296, 465
- Somers, M. W., Mukai, K., & Naylor, T. 1996, *MNRAS*, 278, 845
- Sproats, L. N., Howell, S. B., & Mason, K. O. 1996, *MNRAS*, 282, 1211
- Stiening, R., Skrutskie, M. F., & Capps, R. 1995, *BAAS*, 187, 75.08
- Stolz, B., & Schoembs, R. 1984, *A&A*, 132, 187
- Stover, R. J., Robinson, E. L., & Nather, R. E. 1981, *ApJ*, 248, 696
- Sugano, M., Kosai, H., Alcock, G. E. D., Hurst, G. M., McNaught, R. H., Harrison, T., & Buczynski, D. 1991, *IAU Circ.*, 5222, 1
- Szkody, P. 1987, *ApJS*, 63, 685
- . 1994, *AJ*, 108, 639
- Szkody, P., & Capps, R. W. 1980, *AJ*, 85, 882
- Szkody, P., & Downes, R. A. 1982, *PASP*, 94, 328
- Szkody, P., & Feinswog, L. 1988, *ApJ*, 334, 422
- Szkody, P., & Mateo, M. 1986, *AJ*, 92, 483
- Szkody, P., & Wade, R. A. 1981, *ApJ*, 251, 201
- Thorstensen, J. R. 1997, *PASP*, 109, 1241
- Thorstensen, J. R., & Ringwald, F. A. 1997, *PASP*, 109, 483
- Tovmassian, G. H., Greiner, J., Zickgraf, F. J., Kroll, P., Krautter, J., Thiering, I., Zharykov, S. V., & Serrano, A. 1997, *A&A*, 328, 571
- Venturini, C. C., Lynch, D. K., Rudy, R. J., Mazuk, S. M., & Puetter, R. C. 2000, *BAAS*, 197, 09.06
- Visvanathan, N., Bessell, M. S., & Wickramasinghe, D. T. 1984, *IAU Circ.*, 3923, 2
- Wade, R. A. 1982, *AJ*, 87, 1558
- Warner, B. 1987, *MNRAS*, 227, 23
- . 1995, *Cataclysmic Variables* (Cambridge: Cambridge Univ. Press)
- Webbink, R. F., Livio, M., Truran, J. W., & Orio, M. 1987, *ApJ*, 314, 653
- Weight, A., Evans, A., Naylor, T., Wood, J. H., & Bode, M. F. 1994, *MNRAS*, 266, 761
- Welsh, W. F., Horne, K., & Gomer, R. 1993, *ApJ*, 410, L39
- Whitelock, P., Marang, F., & Feast, M. 2000, *MNRAS*, 319, 728
- Whitelock, P. A., & Munari, U. 1992, *A&A*, 255, 171
- Woodward, C. E., Gehrz, R. D., Jones, T. J., & Lawrence, G. F. 1992, *ApJ*, 384, L41
- Wynn, G. A., King, A. R., & Horne, K. 1995, in *Proc. Cape Workshop on Magnetic CVs*, ed. D. A. H. Buckley & B. Warner (San Francisco: ASP), 196
- Young, P., & Schneider, D. P. 1981, *ApJ*, 247, 960
- Young, P., Schneider, D. P., & Schectman, S. A. 1981, *ApJ*, 245, 1043
- Zuckerman, B., Becklin, E. E., McLean, I. S., & Patterson, J. 1992, *ApJ*, 400, 665